Int. J. Solids Structures Vol. 30, No. 24, pp. 3381–3416, 1993
Printed in Great Britain

0020–7683/93 $6.00+ .00

EFFECTS OF MATERIAL ANISOTROPY AND INHOMOGENEITY ON CAVITATION FOR COMPOSITE INCOMPRESSIBLE ANISOTROPIC NONLINEARLY ELASTIC SPHERES

DEBRA A. POLIGNONE† and CORNELIUS O. HORGAN
Department of Applied Mathematics, University of Virginia, Charlottesville, VA 22903, U.S.A.

(*Received* 31 *December* 1992; *in revised form* 14 *June* 1993)

Abstract—The effects of *material anisotropy* and *inhomogeneity* on void nucleation and growth in incompressible anisotropic nonlinearly elastic solids are examined. A bifurcation problem is considered for a composite sphere composed of two arbitrary homogeneous incompressible nonlinearly elastic materials which are transversely isotropic about the radial direction, and perfectly bonded across a spherical interface. Under a uniform radial tensile dead-load, a branch of radially symmetric configurations involving a traction-free internal cavity bifurcates from the undeformed configuration at sufficiently large loads. Several types of bifurcation are found to occur. Explicit conditions determining the type of bifurcation are established for the general transversely isotropic composite sphere. In particular, if each phase is described by an explicit material model which may be viewed as a generalization of the classic neo-Hookean model to anisotropic materials, phenomena which were not observed for the homogeneous anisotropic sphere nor for the composite neo-Hookean sphere may occur. The stress distribution as well as the possible role of cavitation in preventing interface debonding are also examined for the general composite sphere.

1. INTRODUCTION

Void nucleation and growth in solids is a topic of considerable interest because of the role such phenomena play in fracture and other failure mechanisms [see e.g. Tvergaard (1990) for a review of void growth in metals]. Sudden void formation ("cavitation") in vulcanized rubber has also been observed experimentally by Gent and Lindley (1958) [see also Williams and Schapery (1965)]. A recent review on cavitation in rubber is that of Gent (1990). Nonlinear theories of solid mechanics have been extensively used to model such phenomena. The impetus for much of the current developments has been supplied by the work of Ball (1982). Ball has studied a class of *bifurcation problems* for the equations of nonlinear elasticity which model the appearance of a cavity in the interior of an apparently solid homogeneous isotropic elastic sphere or cylinder once a critical external load is attained. An alternative interpretation for such problems in terms of the sudden rapid growth of a *pre-existing* microvoid has been given by Horgan and Abeyaratne (1986); see also Sivaloganathan (1986a). As pointed out, for example, by Horgan and Abeyaratne (1986), cavitation is an inherently *nonlinear* phenomenon and cannot be modeled using linearized solid mechanics theories.

In the work of Ball (1982) on radially symmetric solutions, bifurcation and stability analyses are carried out for both incompressible and compressible materials. Further studies in the *compressible* case were carried out by Stuart (1985, 1993), Podio-Guidugli *et al.* (1986), Horgan and Abeyaratne (1986), Chung *et al.* (1986), Sivaloganathan (1986a, b), Ertan (1988), Tian-hu (1990), Horgan (1992) and Meynard (1992). Anisotropic compressible materials were considered by Antman and Negrón-Marrero (1987). Other contexts in which cavitation for compressible materials was investigated include consideration of non radially symmetric solutions (James and Spector, 1991), elastodynamics (Pericak-Spector and Spector, 1988) and elastic membrane theory [Haughton (1990), Steigmann (1992); see also Haughton (1986) for incompressible membrane theory]. For *incompressible* materials, finite strain plasticity models were investigated by Chung *et al.* (1987) while the effects of rate dependence were examined by Abeyaratne and Hou (1989). Further studies for incompressible materials were carried out by Chou-Wang and Horgan (1989a), Hou and Zhang (1990) for elastostatics and by Chou-Wang and Horgan (1989b) for elasto-

† Now at Department of Mathematics, University of Tennessee, Knoxville, TN 37996, U.S.A.

dynamics. The effects of material inhomogeneity on cavitation were investigated by Horgan and Pence (1989a, b, c) for incompressible isotropic composite materials. See also Sivaloganathan (1991) for isotropic materials with smoothly varying elastic properties. Void collapse for both incompressible and compressible materials has been examined by Abeyaratne and Hou (1991a). Further work in plasticity was carried out by Hou and Abeyaratne (1992), Huang *et al.* (1991) and Tvergaard *et al.* (1992). The relationship between cavitation and asymmetric instabilities has been discussed by Abeyaratne and Hou (1991b).

In a recent paper (Polignone and Horgan, 1993) the present authors have examined the effects of *material anisotropy* on cavitation for *incompressible* nonlinearly elastic spheres. That investigation was motivated by the work of Antman and Negrón-Marrero (1987) on *compressible* transversely isotropic nonlinearly elastic solids and by the studies of Horgan and Pence (1989a, b, c) on *composite* incompressible nonlinearly elastic spheres with *isotropic* phases. Polignone and Horgan (1993) considered a bifurcation problem for a solid sphere composed of an incompressible homogeneous nonlinearly elastic material which is transversely isotropic about the radial direction. Under a uniform radial tensile dead-load, a branch of radially symmetric configurations involving a traction-free internal cavity bifurcates from the undeformed configuration at sufficiently large loads. Closed form analytic solutions were obtained for a specific material model, which may be viewed as a generalization of the classic neo-Hookean model to anisotropic materials. *In contrast to the situation for a neo-Hookean sphere*, bifurcation was shown to occur locally either to the right (supercritical) or to the left (subcritical), *depending on the degree of anisotropy*. In the latter case, the cavity has finite radius on first appearance. Such a discontinuous change in stable equilibrium configurations is reminiscent of the snap-through buckling phenomenon of structural mechanics. Such dramatic cavitational instabilities ("snap cavitation") were also previously encountered by Antman and Negrón-Marrero (1987) due to anisotropy and by Horgan and Pence (1989a, b, c) due to material inhomogeneity.

The purpose of the present paper is to investigate the combined effects of *anisotropy* and *material inhomogeneity* on cavitation. A more complicated sequence of cavitational instabilities might be expected to occur due to the interaction of these effects and we show that this is indeed the case. In Section 2, we formulate the basic boundary value problem of concern. We consider a composite sphere composed of two incompressible anisotropic nonlinearly elastic phases, each of which is transversely isotropic about the radial direction and perfectly bonded across a spherical interface. The sphere is subjected to a prescribed uniform radial tensile dead-load p_0 on its boundary. In Section 3, it is shown that one solution to this problem, for all values of p_0, corresponds to a trivial homogeneous state in which the sphere remains undeformed but stressed. However, for sufficiently large values of p_0, one has in addition other possible radially symmetric configurations involving an internal traction-free cavity. Such solutions bifurcate from the homogeneous solution at p_{cr}, a critical value of p_0. The possibility for these bifurcated solutions to exist depends *only on the constitutive law for the material at the core* of the composite sphere (Section 4). In Section 4, we also give conditions to determine whether bifurcation is supercritical or subcritical. In Section 5, the stability of the foregoing solutions is examined using an energy minimization approach. For a composite sphere described by a *general* transversely isotropic strain-energy density function, W, the cavitation solutions are shown to be the only stable (radially symmetric) solutions for sufficiently large loads. In Section 6, we present an example which illustrates explicitly the preceding results. The specific anisotropic material model proposed by Polignone and Horgan (1993) for the homogeneous sphere is employed for each phase of the composite, and explicit results are obtained for the relationship $p_0 = p_0(c)$ between the applied tensile load p_0 and the deformed cavity radius c. We also obtain an explicit result for the relationship between the total energy and the deformed cavity radius. We recall that for the isotropic composite sphere considered by Horgan and Pence (1989a, b, c), and the homogeneous anisotropic sphere treated by Polignone and Horgan (1993), when bifurcation at $p_0 = p_{cr}$ occurs locally to the right, a *smooth cavitation* takes place with cavity radius increasing continuously (from zero) as p_0 increases. Here however the situation is quite different. We exhibit *three* possible configurations the sphere

may assume when bifurcation occurs locally to the right. First, a smooth cavitation may take place. Second, a *snap cavitation* may occur in which there is a cavity of *finite* radius upon first appearance at a transition load which is *less* than p_{cr}. Third, the sphere may undergo a smooth cavitation initially, and then experience a discontinuous jump in cavity radius. That is, the cavity radius "snaps" from one finite value to another (larger) finite value at a load p_0 *greater* than p_{cr}. The last two phenomena were not seen in the problems considered by Horgan and Pence (1989a, b, c) and Polignone and Horgan (1993). When bifurcation is to the left, the sphere experiences a snap cavitation so that again a cavity of finite radius appears at a transition load which is less than p_{cr}. In Section 7, the stress distribution is described. When a cavity is nucleated, in the case of smooth cavitation, a predominant stress variation exists in a narrow boundary layer near the cavity wall. Also, the effect of cavitation at the center on possible interface debonding is considered. It is assumed that debonding occurs uniformly whenever the normal stress at the interface reaches a threshold value. A condition on the strain-energy is given so that in a quasi-static loading process, cavitation relieves the interfacial normal stress so that subsequent interfacial debonding is precluded. The boundary layers in the stresses as well as the stress relaxation in the normal stress at the interface subsequent to cavitation are illustrated for the specific material model of Section 6.

It is worth noting here, as was also observed by Antman and Negrón-Marrero (1987) and Polignone and Horgan (1993), that the radial anisotropy considered in those references and in the present paper does indeed arise in technological applications. A striking example occurs in the casting of metals where the temperature gradient in the freezing process induces molecular structure resulting in transverse isotropy about the radial direction [see e.g. Fig. p. 321 of Walker (1956)].

2. PROBLEM FORMULATION

We are concerned with a sphere composed of an incompressible anisotropic nonlinearly elastic material. Using spherical polar coordinates, we denote the interior of the sphere in its undeformed configuration by $D_0 = \{(R, \Theta, \Phi) | 0 \leqslant R < B, 0 < \Theta \leqslant 2\pi, 0 \leqslant \Phi \leqslant \pi\}$. The sphere is subjected to a prescribed uniform radial tensile dead-load of magnitude p_0 on its boundary $R = B$. We assume that the resulting deformation, which takes the point in D_0 with coordinates (R, Θ, Φ) to the point (r, θ, ϕ) in the deformed configuration, is radially symmetric. Thus the deformation has the form $\theta = \Theta$, $\phi = \Phi$,

$$r = r(R) > 0, \quad 0 < R < B, \quad r(0+) \geqslant 0, \tag{1}$$

where $r(R)$ is to be determined.

The deformation gradient tensor $\mathbf{F}$ associated with (1), referred to spherical polar coordinates, is given by

$$\mathbf{F} = \mathrm{diag}(\dot{r}(R), r(R)/R, r(R)/R), \tag{2}$$

where $\dot{r}(R) \equiv (\mathrm{d}r/\mathrm{d}R)$. Incompressibility then requires that $J \equiv \det \mathbf{F} = 1$, which upon integration yields

$$r(R) = (R^3 + c^3)^{1/3}, \tag{3}$$

where $c \geqslant 0$ is a constant to be determined. If it is found that $c = 0$, (3) implies that the body remains a solid sphere in the current configuration. However, if c is found to be positive, then $r(0+) = c > 0$ and so there is a cavity of radius c centered at the origin in the current configuration. In this event, the cavity surface is assumed to be traction-free.

The strain-energy density per unit undeformed volume for an elastic material which is transversely isotropic about the x_1-direction is given by [see e.g. Jaunzemis (1967)]

$$W = W(I_1, I_2, I_3, I_4, I_5), \tag{4}$$

where

$$\left.\begin{aligned} I_1 &= \operatorname{tr} \mathbf{C} \\ I_2 &= \tfrac{1}{2}[(\operatorname{tr} \mathbf{C})^2 - \operatorname{tr} \mathbf{C}^2] \\ I_3 &= \det \mathbf{C} \\ I_4 &= C_{12}^2 + C_{13}^2 \\ I_5 &= C_{11} \end{aligned}\right\}, \tag{5}$$

$\mathbf{C}$ is the right Cauchy–Green deformation tensor $\mathbf{C} = \mathbf{F}^{\mathrm{T}}\mathbf{F}$, and x_i $(i = 1, 2, 3)$ are the usual Cartesian coordinates of a point in the deformed configuration. For incompressible materials, we must have $\mathbf{I}_3 = \mathbf{J}^2 = 1$. The corresponding response equation for the Cauchy stress tensor $\mathbf{T}$ for transversely isotropic incompressible materials is (Jaunzemis, 1967)

$$\mathbf{T} = -p\mathbf{1} + 2(W_1\mathbf{B} - W_2\mathbf{B}^{-1} + W_4\mathbf{M} + W_5\mathbf{N}), \tag{6}$$

where $\mathbf{B}$ is the left Cauchy–Green deformation tensor $\mathbf{B} = \mathbf{F}\mathbf{F}^{\mathrm{T}}$, $\mathbf{1}$ is the unit tensor, p is the unknown hydrostatic pressure associated with the incompressibility constraint $J = 1$, and $W_q = \partial W/\partial I_q$ $(q = 1, 2, 4, 5)$. The deformation tensors $\mathbf{M}$, $\mathbf{N}$ associated with the anisotropy are given by

$$M_{ij} = C_{1\alpha}(F_{i\alpha}F_{j1} + F_{j\alpha}F_{i1}) \quad (\alpha = 2, 3) \tag{7}$$

and

$$N_{ij} = F_{i1}F_{j1}, \tag{8}$$

where $i, j = 1, 2, 3$, and the usual Cartesian tensor notation, with summation over repeated indices, is used. We shall assume that the strain-energy W vanishes in the undeformed state where $I_1 = 3$, $I_2 = 3$, $I_3 = 1$, $I_4 = 0$ and $I_5 = 1$, so that we have the normalization condition

$$W(3, 3, 1, 0, 1) = 0. \tag{9}$$

We also assume that in the undeformed state the initial stress is a hydrostatic pressure, so that (6) gives the further normalization condition

$$W_5(3, 3, 1, 0, 1) = 0. \tag{10}$$

The incompressible material of concern here is assumed to be transversely isotropic about the radial direction, and possibly inhomogeneous in the radial direction as well. The strain-energy density per unit undeformed volume for such an elastic material is denoted by

$$W = W(I_1, I_2, I_3, I_4, I_5; R), \tag{11}$$

where the explicit dependence of W on the radial coordinate R reflects the possible material inhomogeneity. The normalization conditions (9), (10) are now written as

$$W(3, 3, 1, 0, 1; R) = 0 \quad \forall\ R \geqslant 0, \tag{12}$$

and

$$W_5(3, 3, 1, 0, 1; R) = 0 \quad \forall\ R \geqslant 0, \tag{13}$$

respectively. We shall be concerned in what follows with the case of a composite sphere composed of two different transversely isotropic incompressible materials perfectly bonded across the interface $R = A(<B)$. The material properties in each individual phase are

assumed to have smooth radial dependence. Thus $W(I_1, I_2, I_3, I_4, I_5; R)$ is assumed to be smooth on $0 < R < A, A < R < B$ while suffering a jump discontinuity at the interface $R = A$. Observe that, by virtue of (3), the deformation field is continuous at this interface. In the remainder of this section, we proceed formally and assume that W possesses sufficient regularity properties to permit the subsequent analysis.

In (5)–(8) we now let (R, Θ, Φ), (r, θ, ϕ) be associated with the indices $(1, 2, 3)$ and so obtain corresponding to the deformation field (1),

$$\mathbf{C} = \mathbf{B} = \operatorname{diag}(\dot{r}^2, r^2/R^2, r^2/R^2), \tag{14}$$

$$\mathbf{M} = \mathbf{0}, \tag{15}$$

$$\mathbf{N} = \operatorname{diag}(\dot{r}^2, 0, 0) \tag{16}$$

and

$$I_1 = \dot{r}^2 + 2r^2/R^2, \tag{17}$$

$$I_2 = r^4/R^4 + 2\dot{r}^2 r^2/R^2, \tag{18}$$

$$I_3 = \dot{r}^2 r^4/R^4 = 1, \tag{19}$$

$$I_4 = 0, \tag{20}$$

$$I_5 = \dot{r}^2. \tag{21}$$

Substitution from (14)–(16) into (10) yields the nonzero components of the Cauchy stress $\mathbf{T}$ as

$$T_{rr} = -p + 2(\dot{r}^2 W_1 - \dot{r}^{-2} W_2 + \dot{r}^2 W_5) \tag{22}$$

and

$$T_{\theta\theta} = T_{\phi\phi} = -p + 2(\dot{r}^{-1} W_1 - \dot{r} W_2), \tag{23}$$

where the W_t $(t = 1, 2, 5)$ are evaluated at the values of the invariants given by (17)–(21), and we note that W_t is also dependent on the radial coordinate R. The derivatives in (22), (23) are understood to be one-sided derivatives at the material interface $R = A$.

The equilibrium equations, in the absence of body forces, are

$$\operatorname{div} \mathbf{T} = \mathbf{0}, \tag{24}$$

which in the present case reduce to

$$\frac{\partial T_{rr}}{\partial r} + \frac{2}{r}(T_{rr} - T_{\theta\theta}) = 0, \tag{25}$$

$$\frac{1}{r}\frac{\partial T_{\theta\theta}}{\partial \theta} = 0, \tag{26}$$

$$\frac{1}{r \sin\theta}\frac{\partial T_{\phi\phi}}{\partial \phi} = 0. \tag{27}$$

Equation (11), in view of (17)–(21), implies that W and W_q are independent of the angular variables, and thus it follows from (23), (26) and (27) that the pressure $p = p(r)$ only. There may be a jump discontinuity at the interface $R = A$ in $p(r)$. Elsewhere the pressure is assumed sufficiently smooth. Since $r = r(R)$, it is convenient for us to consider $\mathbf{T} = \mathbf{T}(R)$

[and $p = p(R)$] rather than the more conventional $\mathbf{T}(r), p(r)$. The remaining equilibrium equation (25), on using the chain-rule, becomes

$$\frac{dT_{rr}}{dR} + \frac{2\dot{r}}{r}(T_{rr} - T_{\theta\theta}) = 0, \quad \text{on} \quad 0 < R < A, \quad A < R < B. \tag{28}$$

Equation (28) is a first-order nonlinear ordinary differential equation for the pressure $p(R)$. Also for equilibrium, the normal traction component at the material interface must be continuous, i.e.

$$T_{rr}(A-) = T_{rr}(A+). \tag{29}$$

The dead-load boundary condition now requires that

$$T_{rr}(B) = p_0\left[\frac{B}{r(B)}\right]^2, \tag{30}$$

where the constant $p_0 > 0$ is prescribed. We note that the boundary conditions of vanishing shear tractions are satisfied identically.

Thus, the boundary value problem to be solved is the following: *For a prescribed value of the dead-load traction* $\mathrm{p}_0 > 0$, *we seek a pressure field* $\mathrm{p(R)}$ *and a constant* $\mathrm{c} \geqslant 0$ *such that (28)–(30) are satisfied where* $\mathrm{T_{rr}}$, $\mathrm{T_{\theta\theta}}$ *are given by (22), (23), (3). In addition if* $\mathrm{c} > 0$, *then the condition for a traction-free cavity surface*

$$\mathrm{T_{rr}}(0) = 0, \tag{31}$$

must also hold.

3. SOLUTIONS

On using the normalization condition (13), it may readily be shown that one solution of the foregoing problem for all values of p_0 is

$$p(R) = 2[W_1(3,3,1,0,1\,;\,R) - W_2(3,3,1,0,1\,;\,R)] - p_0, \quad c = 0. \tag{32}$$

This corresponds to the trivial homogeneous state of deformation

$$r(R) = R, \tag{33}$$

with corresponding stresses $T_{rr} = T_{\theta\theta} = T_{\phi\phi} = p_0$, so that the sphere remains undeformed under a state of hydrostatic pressure. Note that even though the pressure p given in (32) is in general discontinuous across the interface $R = A$, the corresponding stresses are continuous.

We next describe solutions for which $c > 0$, corresponding to the presence of a traction-free cavity at the origin. We use the notation [cf. Ball (1982) and Horgan and Pence (1989a)]

$$\left.\begin{aligned} v = v(R) \equiv r(R)/R &= \left(1 + \frac{c^3}{R^3}\right)^{1/3} \\ [v^{-2} = \dot{r}] & \end{aligned}\right\}, \tag{34}$$

and thus rewrite the invariants (17)–(21) as

$$\left.\begin{aligned} I_1 &= v^{-4}+2v^2 \\ I_2 &= v^4+2v^{-2} \\ I_3 &= 1 \\ I_4 &= 0 \\ I_5 &= v^{-4} \end{aligned}\right\}. \tag{35}$$

Following the approach of Horgan and Pence (1989a) and Polignone and Horgan (1993), we rewrite the differential equation (28) in the form

$$\frac{\mathrm{d}}{\mathrm{d}R}\{2[v^{-4}W_1|_R - v^4 W_2|_R + v^{-4}W_5|_R] - p(R)\}$$
$$+\frac{4v^{-3}}{R}[(v^{-4}-v^2)W_1|_R + (v^{-2}-v^4)W_2|_R + v^{-4}W_5|_R] = 0 \quad \text{on} \quad 0 < R < A,\ A < R < B. \tag{36}$$

On integration of (36), we have

$$p(R) - p(0) = 2\{v^{-4}(R)(W_1+W_5)|_R - v^4(R)W_2|_R\} + 4J(R), \quad 0 < R < A, \tag{37}$$

and

$$p(R) - [p]_{A-}^{A+} - p(0) = 2\{v^{-4}(R)(W_1+W_5)|_R - v^4(R)W_2|_R$$
$$-v^{-4}(A)[W_1+W_5]_{A-}^{A+} + v^4(A)[W_2]_{A-}^{A+}\} + 4J(R), \quad A < R < B, \tag{38}$$

where

$$J(R) = \int_0^R [(v^{-7}(s) - v^{-1}(s))W_1|_s + (v^{-5}(s) - v(s))W_2|_s + v^{-7}(s)W_5|_s]\frac{\mathrm{d}s}{s}, \quad 0 < R < B, \tag{39}$$

and $[f(s)]_{A-}^{A+} = f(A+) - f(A-)$. In (36)–(39) the W_l $(l = 1, 2, 5)$ are evaluated at the values of the invariants given by (35), and we have used the notation

$$W_l|_s = W_l(v^{-4}(s) + 2v^2(s), v^4(s) + 2v^{-2}(s), 1, 0, v^{-4}(s);\ s). \tag{40}$$

On substitution into (22), and using (37), the radial stress becomes

$$T_{rr}(R) = -p(0) - 4J(R), \quad 0 < R < A, \tag{41}$$

$$T_{rr}(R) = -p(0) - [p]_{A-}^{A+} + 2\{v^{-4}(A)[W_1+W_5]_{A-}^{A+} - v^4(A)[W_2]_{A-}^{A+}\} - 4J(R), \quad A < R < B. \tag{42}$$

The interface condition (29) now shows that

$$-[p]_{A-}^{A+} + 2\{v^{-4}(A)[W_1+W_5]_{A-}^{A+} - v^4(A)[W_2]_{A-}^{A+}\} = 0, \tag{43}$$

so that (42) becomes

$$T_{rr}(R) = -p(0) - 4J(R), \quad A < R < B. \tag{44}$$

The traction-free cavity surface condition (31), together with (41) and $J(0) = 0$, now yield $p(0) = 0$, so that

$$T_{rr}(R) = -4J(R), \quad 0 < R < B. \tag{45}$$

Finally, by virtue of (45) and (34), we see that the dead-load boundary condition (30) at the outer surface $R = B$ is satisfied if

$$-4J(B) = p_0[v(B)]^{-2}. \tag{46}$$

As in Horgan and Pence (1989a) and Polignone and Horgan (1993), the condition (46) may be written compactly on utilizing the $s \to v$ change of variables in the integral (39). Introducing the function

$$\hat{W}(x; y) = W(x^{-4}+2x^2, x^4+2x^{-2}, 1, 0, x^{-4}; y), \tag{47}$$

and adopting the notation

$$\hat{W}_1(x; y) = \frac{\partial}{\partial x}\hat{W}(x; y), \tag{48}$$

as in Horgan and Pence (1989a), it follows from the arguments given by Polignone and Horgan (1993) that one may write (46) as

$$p_0 = \left(1+\frac{c^3}{B^3}\right)^{2/3} \int_{[1+(c^3/B^3)]^{1/3}}^{\infty} \frac{\hat{W}_1\left(v; \dfrac{c}{(v^3-1)^{1/3}}\right)}{v^3-1}\,\mathrm{d}v, \quad c > 0. \tag{49}$$

We remark that (49), here established for the anisotropic composite sphere, has the same structure as the analogous relation for the isotropic composite sphere [see eqn (2.23) of Horgan and Pence (1989a)]. As discussed in that reference, the integrand in this equation is, in general, discontinuous at the interface $v = [1+(c^3/A^3)]^{1/3}$. Equation (49) was first established in Ball (1982) for the case of the homogeneous isotropic sphere [see eqn (5.18) of Ball (1982); see also Sivaloganathan (1991) for the inhomogeneous case]. Thus, for a given dead-load p_0, solutions involving a traction-free internal cavity of radius c exist provided that c is a positive root of (49). The associated pressure field is given by

$$p(R) = 2[v^{-4}(R)(W_1+W_5)|_R - v^4(R)W_2|_R] + 4J(R), \quad \text{on} \quad 0 < R < A, \quad A < R < B. \tag{50}$$

In summary, we have seen that for all values of the applied dead-load traction p_0, one obtains the trivial solution (32) corresponding to the homogeneous state of deformation (33). Moreover, if positive roots c of (49) exist, then one obtains the *additional* solutions involving a traction-free internal cavity described above.

4. THE CRITICAL LOAD AND BIFURCATION

Henceforth we confine attention to a composite sphere composed of two *homogeneous* anisotropic phases. To remove the explicit radial dependence from the strain-energy, we now write $W = W(I_1, I_2, I_3, I_4, I_5; \mathrm{R})$ for the composite sphere as

$$\begin{aligned} W &= W^1(I_1, I_2, I_3, I_4, I_5), \quad 0 \leqslant R < A, \\ W &= W^2(I_1, I_2, I_3, I_4, I_5), \quad A < R \leqslant B. \end{aligned} \tag{51}$$

Using the definitions in (47), (48) and (51), and noting that the second argument in (48) is no longer required, we rewrite (49) as

$$p_0 = \left(1+\frac{c^3}{B^3}\right)^{2/3}\left[\int_{[1+(c^3/A^3)]^{1/3}}^{\infty} \frac{\hat{W}_1^1(v)}{v^3-1}\,dv + \int_{[1+(c^3/B^3)]^{1/3}}^{[1+(c^3/A^3)]^{1/3}} \frac{\hat{W}_1^2(v)}{v^3-1}\,dv\right], \quad c>0. \tag{52}$$

The *critical load* p_{cr} at which an internal cavity may be initiated is then found by formally letting $c \to 0+$ in (52), and so

$$p_{cr} = \int_1^{\infty} \frac{\hat{W}_1^1(v)}{v^3-1}\,dv. \tag{53}$$

Since the integral in (53) is improper, p_{cr} may or may not be finite, and thus cavitation may or may not take place. We also see from (53) that the finiteness of p_{cr} and its value depend *only upon the material at the core of the composite sphere*. Such a result was also obtained in Horgan and Pence (1989b) for a composite sphere with isotropic phases [see also Sivaloganathan (1991) for a more general result for inhomogeneous isotropic materials]. In Section 5, we derive an alternative formula for the critical load involving the strain-energy function $\hat{W}^1(v)$ instead of its derivative, as in (53).

As regards the lower limit in (53), it is readily verified [see Polignone and Horgan (1993)] that

$$\frac{d\hat{W}^1(1)}{dv} = 0, \quad \frac{d^2\hat{W}^1(1)}{dv^2} = 4(\bar{\beta}^1 - \mu_T^1 + 4\mu_L^1), \tag{54}$$

where $\bar{\beta}^1$, μ_T^1, μ_L^1 are elastic constants associated with infinitesimal deformations of the transversely isotropic material at the core. Thus by l'Hopital's rule, the limit of the integrand in (53) is finite as $v \to 1$. Thus, the finiteness of p_{cr} depends on the behavior of $\hat{W}^1(v)$ for *large* values of the stretch v. For example, suppose that the strain-energy density $\hat{W}^1$ can be written in the form

$$\hat{W}^1(v) = a_{-m}v^{-m} + \cdots + a_{-1}v^{-1} + a_0 + a_1 v + \cdots + a_n v^n, \quad m,n \geq 0, \quad m+n>0. \tag{55}$$

Then, it can be easily shown that p_{cr} is finite if

$$n < 3 \tag{56}$$

[cf. Chou-Wang and Horgan (1989a) and Polignone and Horgan (1993)]. For more general W^1, the finiteness of p_{cr} in (53) also requires restrictions on the rate of growth of W^1 for large stretch.

We now consider the local character of the bifurcation at $p_0 = p_{cr}$ by analysing the curve $p_0 = p_0(c)$, given by (49), for small values of c. We first introduce the dimensionless parameters

$$\rho = \frac{c}{B}, \quad \alpha = \frac{B}{A}, \quad (\alpha > 1) \tag{57}$$

and define

$$p_0(c) \equiv p_0^*(\rho^3) = (1+\rho^3)^{2/3}\left[\int_{(1+\alpha^3\rho^3)^{1/3}}^{\infty} \frac{\hat{W}_1^1(v)}{v^3-1}\,dv + \int_{(1+\rho^3)^{1/3}}^{(1+\alpha^3\rho^3)^{1/3}} \frac{\hat{W}_1^2(v)}{v^3-1}\,dv\right]. \tag{58}$$

A Taylor expansion of (58) about $\rho^3 = 0$ shows that

$$p_0 = p_{cr} + k\rho^3 + o(\rho^3) \quad \text{as} \quad \rho^3 \to 0, \tag{59}$$

where

$$k = \lim_{\rho^3 \to 0} \mathrm{d}p_0^*/\mathrm{d}\rho^3. \tag{60}$$

From (58) one obtains

$$k = \tfrac{2}{3}p_{\mathrm{cr}} - \tfrac{1}{3}\alpha^3 \lim_{v \to 1} \frac{\mathrm{d}\hat{W}^1/\mathrm{d}v}{v^3 - 1} + \tfrac{1}{3}(\alpha^3 - 1) \lim_{v \to 1} \frac{\mathrm{d}\hat{W}^2/\mathrm{d}v}{v^3 - 1}. \tag{61}$$

On using l'Hopital's rule and defining

$$f = \alpha^{-3}, \quad 0 < f < 1, \tag{62}$$

as the volume fraction of the core material to the total material, we write k as

$$k = \frac{2}{3}\left[p_{\mathrm{cr}} - \tfrac{1}{6} f^{-1} \frac{\mathrm{d}^2\hat{W}^1(1)}{\mathrm{d}v^2} + \tfrac{1}{6}(f^{-1} - 1) \frac{\mathrm{d}^2\hat{W}^2(1)}{\mathrm{d}v^2} \right], \tag{63}$$

where the quantities $\mathrm{d}^2\hat{W}^i(1)/\mathrm{d}v^2$ $(i = 1, 2)$, are positive and finite, and each can be written in terms of the associated infinitesimal elastic moduli (see Appendix A). We see from (59) that if $k > 0$, bifurcation is locally to the right (supercritical) while if $k < 0$, bifurcation is locally to the left (subcritical). Equations corresponding to (59) and (63) were also determined by Horgan and Pence (1989b) for the case of an isotropic composite sphere, as well as by Polignone and Horgan (1993) for the case of a homogeneous transversely isotropic sphere. We now make the further definitions

$$K = \frac{k}{\mathrm{d}^2\hat{W}^1(1)/\mathrm{d}v^2}, \quad \omega = \frac{\mathrm{d}\hat{W}^2(1)/\mathrm{d}v^2}{\mathrm{d}^2\hat{W}^1(1)/\mathrm{d}v^2},$$

$$\hat{p}_{\mathrm{cr}} = \frac{p_{\mathrm{cr}}}{\mathrm{d}^2\hat{W}^1(1)/\mathrm{d}v^2}, \quad \hat{p} = \frac{p_0}{\mathrm{d}^2\hat{W}^1(1)/\mathrm{d}v^2}, \tag{64}$$

so that

$$K = \tfrac{2}{3}[\hat{p}_{\mathrm{cr}} - \tfrac{1}{6} f^{-1} + \tfrac{1}{6}(f^{-1} - 1)\omega]. \tag{65}$$

Letting $f \to 1$ in (65), we obtain the value of K appropriate to the homogeneous transversely isotropic sphere composed of the core material, namely

$$K_{\mathrm{h}} \equiv \tfrac{2}{3}(\hat{p}_{\mathrm{cr}} - \tfrac{1}{6}). \tag{66}$$

In contrast to the case for a homogeneous *isotropic* sphere for which $K_{\mathrm{h}} > 0$ so that bifurcation is only to the right [see Section 5.2 of Ball (1982) or eqn (25) of Horgan and Pence (1989b)], it was shown by Polignone and Horgan (1993) that for the *anisotropic* sphere, bifurcation can occur either to the right *or* to the left. Thus, for the anisotropic sphere, K_{h} can be either positive or negative.

Returning to (65), we now discuss the circumstances which determine whether the bifurcation for the composite sphere is locally to the right or to the left. It is convenient to

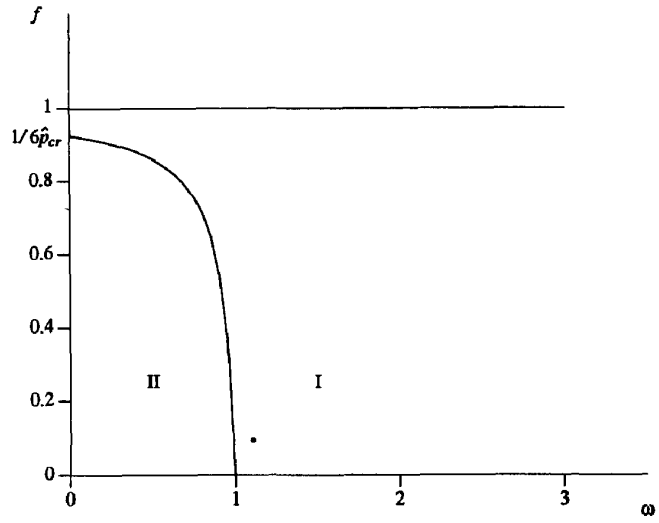

Fig. 1. Semi-infinite strip

$$0 < f = \frac{A^3}{B^3} < 1, \quad \omega = \frac{d^2\hat{W}^2(1)/dv^2}{d^2\hat{W}^1(1)/dv^2} = \frac{\mu_2(3+4a_2)}{\mu_1(3+4a_1)} > 0.$$

For parameter pairs (ω, f) in region I, the bifurcation occurs to the right, while in region II, bifurcation occurs to the left. For the curve shown, $p_{cr}/\mu_1 = 4(3+4a_1)\hat{p}_{cr}$, $a_1 = 0.157$, $\hat{p}_{cr} = 0.18$. Figure 1 corresponds to the case in which bifurcation for the *homogeneous sphere composed of the core material would be to the right* ($\hat{p}_{cr} > 1/6$). The point shown in region I is the parameter pair associated with Fig. 3.

treat these cases with reference to the schematic diagrams in Figs 1 and 2. Figure 1 corresponds to the case in which bifurcation for the *homogeneous sphere composed of the core material would be to the right*, and Fig. 2 to the case in which such a sphere would bifurcate to the *left*. In these figures, the semi-infinite strips $0 < f < 1, 0 < \omega < \infty$, are divided into two regions, I, II, by the curve

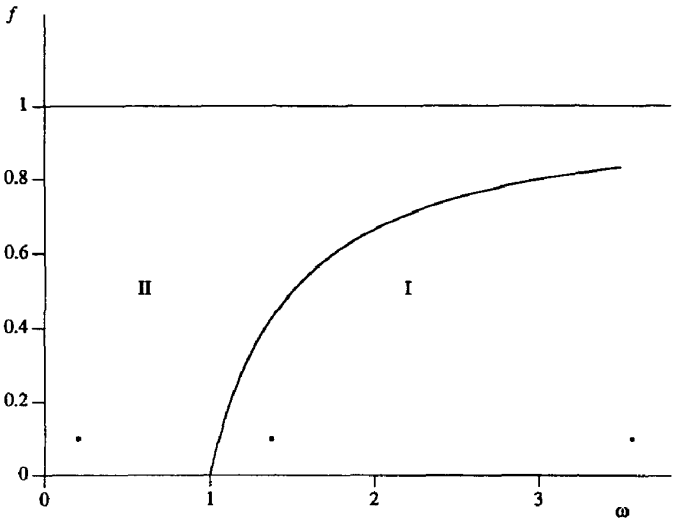

Fig. 2. Semi-infinite strip

$$0 < f = \frac{A^3}{B^3} < 1, \quad \omega = \frac{d^2\hat{W}^2(1)/dv^2}{d^2\hat{W}^1(1)/dv^2} = \frac{\mu_2(3+4a_2)}{\mu_1(3+4a_1)} > 0.$$

For parameter pairs (ω, f) in region I, bifurcation occurs to the right, while in region II, bifurcation occurs to the left. Figure 2 corresponds to the case in which bifurcation for the *homogeneous sphere composed of the core material would be to the left* ($\hat{p}_{cr} < 1/6$). The point shown in region II is the parameter pair (ω, f) associated with Fig. 4, while the points in region I, ordered with increasing ω, are the parameter pairs associated with Figs 6(a) and 5(a), respectively.

$$f(\omega) = \frac{\omega - 1}{\omega - 6\hat{p}_{cr}} \tag{67}$$

on which $K = 0$. When $K_h > 0$ (Fig. 1), the curve (67) is monotone *decreasing* on the region of interest, and when $K_h < 0$ (Fig. 2), the curve (67) is monotone *increasing* with $f(\omega) \to 1$ as $\omega \to \infty$. In view of the remark made above following (66), we note that *there is no diagram analogous to* Fig. 2 for the composite *isotropic* sphere considered in Horgan and Pence (1989a, b, c). In both Figs 1 and 2, if (ω, f) lies in region I, then $K > 0$ and so bifurcation for the composite sphere is to the right, while if (ω, f) lies in region II, then $K < 0$ and so bifurcation is to the left.

As in Horgan and Pence (1989b), we may discuss these diagrams with reference to a composite sphere of either fixed geometric properties together with varying material properties or vice versa. We first consider Fig. 1 so that $K_h > 0$ ($\Rightarrow \hat{p}_{cr} > 1/6$). Taking the former view, we see that for

$$f \geqslant \frac{1}{6\hat{p}_{cr}} \tag{68}$$

bifurcation is always to the right. *Thus, if the volume fraction of the core to the total volume exceeds* $1/6\hat{p}_{cr}$, *bifurcation is locally to the right regardless of the material properties of the outer material.* Taking the latter view, we also see that for $\omega \geqslant 1$, i.e. for

$$\frac{d^2\hat{W}^2(1)}{dv^2} \geqslant \frac{d^2\hat{W}^1(1)}{dv^2} \tag{69}$$

bifurcation is always to the right. As discussed in Appendix A, one has

$$\frac{d^2\hat{W}(1)}{dv^2} = 4(\bar{\beta} - \mu_T + 4\mu_L), \tag{70}$$

where $\bar{\beta}$, μ_T, μ_L are elastic constants associated with infinitesimal deformations of the transversely isotropic material at hand [cf. $(54)_2$]. In Appendix A, it is shown that

$$\bar{E} = \bar{\beta} - \mu_T + 4\mu_L, \tag{71}$$

where $\bar{E}$ is Young's modulus in the direction of anisotropy, i.e. the radial direction. *Thus, from* (69) *to* (71), *if the material in the surrounding shell is stiffer in tension in the radial direction than the core material,* $(\bar{E}^2 \geqslant \bar{E}^1)$, *bifurcation is to the right irrespective of geometry.*

On the other hand, the condition for bifurcation to the left requires *both* geometric and material restrictions. These may be written as

$$f < \frac{\omega - 1}{\omega - 6\hat{p}_{cr}} \quad \text{and} \quad \omega < 1. \tag{72}$$

Thus, the occurrence of bifurcation to the left in a composite sphere corresponding to Fig. 1 requires *a sufficiently small core surrounded by a shell of sufficiently compliant material.*

We next consider the similar implications in Fig. 2, so that now the core material alone will undergo bifurcation to the left ($K_h < 0 \Rightarrow \hat{p}_{cr} < 1/6$). In contrast to the case of Fig. 1, we cannot determine a single condition for bifurcation to the right to occur. Thus, we must have

$$f < \frac{\omega - 1}{\omega - 6\hat{p}_{cr}} \quad \text{and} \quad \omega > 1. \tag{73}$$

In other words, the occurrence of bifurcation to the right in a composite sphere corresponding to Fig. 2 requires *a sufficiently small core surrounded by a shell of sufficiently stiff material.*

The situation for bifurcation to the left is much different. Although we can draw no conclusions based on geometric properties alone, we can deduce that for

$$\omega \leqslant 1 (\Rightarrow \bar{E}^2 \leqslant \bar{E}^1), \tag{74}$$

bifurcation is always to the left. *Thus, if the material in the surrounding shell is more compliant in tension in the radial direction than the core material, bifurcation is to the left irrespective of geometry.*

Finally from Fig. 2, if

$$\omega > 1 (\Rightarrow \bar{E}^2 > \bar{E}^1) \tag{75}$$

and

$$f > \frac{\omega - 1}{\omega - 6\hat{p}_{cr}}, \tag{76}$$

we also have a bifurcation to the left occurring. Thus, bifurcation to the left in a composite sphere corresponding to Fig. 2 is also possible provided there is *a sufficiently large core surrounded by a shell of sufficiently stiff material.*

The foregoing results may be summarized as follows:

(i) if the core material alone would undergo a bifurcation to the $\left\{\begin{matrix}\text{right}\\ \text{left}\end{matrix}\right\}$, then the composite sphere will also bifurcate to the $\left\{\begin{matrix}\text{right}\\ \text{left}\end{matrix}\right\}$ provided the surrounding shell is $\left\{\begin{matrix}\text{stiffer}\\ \text{more compliant}\end{matrix}\right\}$ in tension in the radial direction than the core material;

(ii) if the core material alone would undergo a bifurcation to the $\left\{\begin{matrix}\text{right}\\ \text{left}\\ \text{left}\end{matrix}\right\}$, then the composite sphere will bifurcate to the $\left\{\begin{matrix}\text{left}\\ \text{right}\\ \text{left}\end{matrix}\right\}$ provided there is a sufficiently $\left\{\begin{matrix}\text{small}\\ \text{small}\\ \text{large}\end{matrix}\right\}$ core surrounded by a shell which is $\left\{\begin{matrix}\text{more compliant}\\ \text{stiffer}\\ \text{stiffer}\end{matrix}\right\}$ in tension in the radial direction than the core material;

(iii) if the core material alone would undergo a bifurcation to the right, the composite sphere will also bifurcate to the right provided the volume fraction of the core to the total volume exceeds $1/6\hat{p}_{cr}$.

We conclude this section by again emphasizing that the behavior of the composite sphere is highly dependent upon the core material. Whether cavitation will or will not take place depends *solely* on the core material. The value of the critical load depends only on the core material. Furthermore, material properties of the core alone determine which of the schematic diagrams (Fig. 1 or Fig. 2) applies.

5. ENERGY AND STABILITY OF SOLUTIONS

To examine the stability of the cavitation solutions, we now carry out an energy analysis. This will be done for the *general* transversely isotropic strain-energy W described by (11). The total energy associated with any radially symmetric equilibrium configuration of the body is given by

$$E(c) = 4\pi \int_0^B W|_R R^2 \, dR - 4\pi B^2 p_0 [r(B) - B], \tag{77}$$

where notation analogous to (40) is employed. For the trivial solution (32) with deformation (33), we have

$$E(0) = 0 \tag{78}$$

on using the normalization (12). We now consider (77) to hold for all values of $c \geqslant 0$, and thus seek values of $c \geqslant 0$ that, for a given $p_0 > 0$, minimize the extended energy function $E(c)$.

Recalling the notation (47), (34), we may write eqn (77) as

$$E(c) = 4\pi c^3 \int_{(1+c^3/B^3)^{1/3}}^{\infty} v^2 (v^3 - 1)^{-2} \hat{W}\left(v; \frac{c}{(v^3-1)^{1/3}}\right) dv - 4\pi B^2 p_0 [r(B) - B], \quad c > 0. \tag{79}$$

Henceforth, for simplicity of notation, we omit the explicit dependence of $\hat{W}$ on its second argument. Upon introduction of the dimensionless quantity

$$\Sigma = \frac{E}{(4/3)\pi B^3 \, d^2 \hat{W}^1(1)/dv^2}, \tag{80}$$

and using (51), (57) and (3), we rewrite (79) as

$$\frac{d^2 \hat{W}^1(1)}{dv^2} \Sigma(\rho) = 3\rho^3 \left\{ \int_{(1+\rho^3)^{1/3}}^{(1+\alpha^3\rho^3)^{1/3}} v^2 (v^3-1)^{-2} \hat{W}^2(v) \, dv + \int_{(1+\alpha^3\rho^3)^{1/3}}^{\infty} v^2 (v^3-1)^{-2} \hat{W}^1(v) \, dv \right\} - 3p_0 [(1+\rho^3)^{1/3} - 1]. \tag{81}$$

We now let

$$\Sigma(\rho) = \frac{1}{d^2 \hat{W}^1(1)/dv^2} [\Phi(\rho) + p_0 \Psi(\rho)], \quad \rho \geqslant 0, \tag{82}$$

where

$$\Phi(\rho) = 3\rho^3 \left\{ \int_{(1+\rho^3)^{1/3}}^{(1+\alpha^3\rho^3)^{1/3}} \frac{v^2 \hat{W}^2(v)}{(v^3-1)^2} \, dv + \int_{(1+\alpha^3\rho^3)^{1/3}}^{\infty} \frac{v^2 \hat{W}^1(v)}{(v^3-1)^2} \, dv \right\} \tag{83}$$

and

$$\Psi(\rho) = -3[(1+\rho^3)^{1/3} - 1]. \tag{84}$$

We thus state the energy minimization problem as: *for fixed* $p_0 > 0$, *we seek those values of* $\rho \geqslant 0$ *that minimize* $\Sigma(\rho)$.

We first examine the end-point $\rho = 0$ where $\Sigma(0) = 0$. It is shown in Appendix B that

$$\dot{\Sigma}(0+) = \ddot{\Sigma}(0+) = 0, \quad \dddot{\Sigma}(0+) = 6(\hat{p}_{cr} - \hat{p}), \tag{85}$$

where the superposed dot denotes differentiation with respect to ρ, and $\hat{p}_{cr}$, $\hat{p}$ are given by (64) and (53). Thus $\rho = 0$ is a local minimum if $\hat{p} < \hat{p}_{cr}(p_0 < p_{cr})$ and a local maximum if $\hat{p} > \hat{p}_{cr}(p_0 > p_{cr})$. Observe that

$$\rho = 0, \quad p_0 > 0, \tag{86}$$

corresponds to the trivial solution (32).

We now consider the possible existence of internal extrema and thus seek values of $\rho > 0$ for which

$$\dot{\Sigma}(\rho) = 0 \quad \text{and so} \quad \dot{\Phi}(\rho) + p_0 \dot{\Psi}(\rho) = 0. \tag{87}$$

From (84), $\dot{\Psi}(\rho) < 0$ for $\rho > 0$ so that (87) may be written as

$$p_0 = -\frac{\dot{\Phi}(\rho)}{\dot{\Psi}(\rho)}, \quad \rho > 0. \tag{88}$$

We note that the expression (88) for $p_0(\rho)$ derived from energy considerations can be shown to be identical to the expression (49) determined directly in Section 3. Thus, as expected, the extremals provided by (88) correspond to equilibrium solutions with an internal cavity.

We next analyse the dimensionless energy $\Sigma(\rho)$ given by (82)–(84) near $\rho^3 = 0$. A straightforward calculation shows that

$$\Psi(\rho) \equiv \Psi^*(\rho^3) = -\rho^3 + \tfrac{1}{3}\rho^6 + O(\rho^9) \quad \text{as} \quad \rho^3 \to 0. \tag{89}$$

On using (89) and (59), the last term in (82) has the asymptotic expression

$$p_0(\rho)\Psi(\rho) = -p_{cr}\rho^3 + (\tfrac{1}{3}p_{cr} - k)\rho^6 + O(\rho^9) \quad \text{as} \quad \rho^3 \to 0, \tag{90}$$

where k is given by (63). We next consider the Taylor expansion

$$\Phi(\rho) \equiv \Phi^*(\rho^3) = \Phi^*(0) + \frac{d\Phi^*}{d\rho^3}(0)\rho^3 + \frac{1}{2}\frac{d^2\Phi^*}{d(\rho^3)^2}(0)\rho^6 + O(\rho^9) \quad \text{as} \quad \rho^3 \to 0. \tag{91}$$

It is easily seen that

$$\Phi^*(0) = 0. \tag{92}$$

This follows from the fact that $\Sigma(0) = 0$ and so from (82), $\Phi(0) + p_0\Psi(0) = 0$; however, (84) implies that $\Psi(0) = 0$, so that (92) must hold.

Now, differentiating (83) we obtain

$$\frac{d\Phi^*}{d\rho^3} = 3\left\{\int_{(1+\rho^3)^{1/3}}^{(1+\alpha^3\rho^3)^{1/3}} \frac{v^2\hat{W}^2(v)}{(v^3-1)^2}\,dv + \int_{(1+\alpha^3\rho^3)^{1/3}}^{\infty} \frac{v^2\hat{W}^1(v)}{(v^3-1)^2}\,dv\right\} + \frac{1}{\rho^3}$$
$$\times \{\alpha^{-3}(\hat{W}^2(v) - \hat{W}^1(v))|_{v(A)=(1+\alpha^3\rho^3)^{1/3}} - \hat{W}^2(v)|_{v(B)=(1+\rho^3)^{1/3}}\}, \tag{93}$$

so that

$$\frac{d\Phi^*}{d\rho^3}(0) = 3\int_1^\infty \frac{v^2}{(v^3-1)^2}\hat{W}^1(v)\,dv + \lim_{\rho^3\to 0}\frac{\alpha^{-3}[\hat{W}^2((1+\alpha^3\rho^3)^{1/3}) - \hat{W}^1((1+\alpha^3\rho^3)^{1/3})] - \hat{W}^2((1+\rho^3)^{1/3})}{\rho^3}. \quad (94)$$

Integrating the first term on the right-hand side by parts gives

$$\int_1^\infty 3v^2(v^3-1)^{-2}\hat{W}^1(v)\,dv = \lim_{v\to 1}\frac{\hat{W}^1(v)}{v^3-1} - \lim_{v\to\infty}\frac{\hat{W}^1(v)}{v^3-1} + \int_1^\infty \frac{\hat{W}_1^1(v)}{v^3-1}\,dv, \quad (95)$$

where we note from (53) that the last term in the above equation is p_{cr}. Since $\hat{W}^i(1) = 0$ $(i = 1, 2)$ from (12) and (47), using l'Hopital's rule and $(54)_1$ shows that the first term on the right in (95) is zero. Also, for a finite p_{cr}, i.e. for cavitation to take place, we must have

$$\hat{W}^1(v) = O(v^n), \quad n < 3, \quad \text{as} \quad v \to \infty. \quad (96)$$

Thus, the second term on the right in (95) is also zero so that we arrive at the following *alternative formula for the critical load* [when the strain-energy satisfies the growth assumption (96)]:

$$\int_1^\infty \frac{3v^2}{(v^3-1)^2}\hat{W}^1(v)\,dv = \int_1^\infty \frac{\hat{W}_1^1(v)}{v^3-1}\,dv \equiv p_{cr}. \quad (97)$$

Now, the limit in (94) is zero by arguments similar to those used following eqn (95). Thus, on using the formula (97) for the critical load, (94) reduces to

$$\frac{d\Phi^*}{d\rho^3}(0) = p_{cr}. \quad (98)$$

We next differentiate (93) and obtain

$$\frac{d^2\Phi^*}{d(\rho^3)^2} = \frac{1}{3}\left\{\frac{(\hat{W}_1^2(v) - \hat{W}_1^1(v))|_{v(A)=(1+\alpha^3\rho^3)^{1/3}}}{\rho^3(1+\alpha^3\rho^3)^{2/3}} - \frac{\hat{W}_1^2(v)|_{v(B)=(1+\rho^3)^{1/3}}}{\rho^3(1+\rho^3)^{2/3}}\right\}, \quad (99)$$

so that taking the limit as $\rho^3 \to 0$ and applying l'Hopital's rule gives

$$\frac{d^2\Phi^*}{d(\rho^3)^2}(0) = \frac{1}{9}\left\{\alpha^3\left(\frac{d^2\hat{W}^2}{dv^2}(1) - \frac{d^2\hat{W}^1}{dv^2}(1)\right) - \frac{d^2\hat{W}^2}{dv^2}(1)\right\}. \quad (100)$$

Combining (91), (92), (98), (100) and (62) then gives

$$\Phi^*(\rho^3) = p_{cr}\rho^3 + \frac{1}{18}\left\{f^{-1}\left(\frac{d^2\hat{W}^2}{dv^2}(1) - \frac{d^2\hat{W}^1}{dv^2}(1)\right) - \frac{d^2\hat{W}^2}{dv^2}(1)\right\}\rho^6 + O(\rho^9) \quad \text{as} \quad \rho^3 \to 0. \quad (101)$$

Finally, using (90) and (101) in (82), we obtain

$$\Sigma(\rho) \equiv \Sigma^*(\rho^3) = -\tfrac{1}{2}K\rho^6 + O(\rho^9) \quad \text{as} \quad \rho^3 \to 0, \quad (102)$$

where K is given by (65). The above result, which holds for a composite sphere consisting of two *general* homogeneous transversely isotropic phases, generalizes those found previously by Horgan and Pence (1989a) and Polignone and Horgan (1993). Thus, recalling

the results at the end of Section 4, where the curve (88) [or equivalently (52)] was shown to bifurcate from the trivial solution (86) at the point $\rho = 0$, $p_0 = p_{cr}$, (102) shows that $\Sigma < 0$ on this curve near $\rho = 0$ if the bifurcation is to the right ($K > 0$) and $\Sigma > 0$ if the bifurcation is to the left ($K < 0$). We have thus established, in general, all of the energy results which were employed for the specific material model in Horgan and Pence (1989a) to obtain Properties A and B, which we now restate for convenience:

Property A: The curve $\hat{p} = \hat{p}(\rho)$ is a locus of local *minima* of $\Sigma(\rho)$ *for fixed* $\hat{p}$ whenever $d\hat{p}/d\rho > 0$, and is a locus of local *maxima* of $\Sigma(\rho)$ *for fixed* $\hat{p}$ whenever $d\hat{p}/d\rho < 0$.

Property B: On the curve $\hat{p} = \hat{p}(\rho)$, the values of $\Sigma(\rho)$ are *decreasing* with ρ whenever $d\hat{p}/d\rho > 0$ and are *increasing* with ρ whenever $d\hat{p}/d\rho < 0$.

With the above results we have that, in general, where the curve $\hat{p} = \hat{p}(\rho)$ is monotone decreasing, the cavitated solution is unstable, and where $\hat{p} = \hat{p}(\rho)$ is monotone increasing, the cavitated solution is stable. If there exist two stable solutions corresponding to a particular load, we say that a solution is *absolutely stable* (AS) if it provides the absolute minimum for Σ and is *metastable* (MS) if it provides a local minimum for Σ which is not the absolute minimum. In cases such as this, there may be a discontinuous transition in cavity radius in moving from one stable solution to another. The transition between metastability and absolute stability will be addressed more completely in the illustrative example considered in the following section.

6. ILLUSTRATIVE EXAMPLE

In this section, we illustrate the foregoing results for a specific material model. We consider a composite sphere whose phases are described by a transversely isotropic strain-energy density function proposed by Polignone and Horgan (1993). Thus, we take

$$W = \begin{cases} \dfrac{\mu_1}{2}[(I_1-3)+a_1(I_5^2-2I_5+1)], & 0 \leqslant R < A, \\ \dfrac{\mu_2}{2}[(I_1-3)+a_2(I_5^2-2I_5+1)], & A < R \leqslant B, \end{cases} \tag{103}$$

where I_1, I_5 are given by (17), (21), the μ_i ($i = 1, 2$) are positive constants, and the a_i with $0 \leqslant a_i \leqslant 5.0$ ($i = 1, 2$) are dimensionless parameters which serve as measures of the degree of anisotropy in the respective phases. When $a_1 = 0$, $a_2 = 0$, one recovers the neo-Hookean composite sphere treated by Horgan and Pence (1989a, b, c). The response to certain basic homogeneous deformations of a homogeneous material modeled by a strain-energy of the form (103) is discussed in Polignone and Horgan (1993). Recalling the notation (34), (47), and using (35), we rewrite (103) as

$$\hat{W}(v) = \begin{cases} \hat{W}^1(v) = \dfrac{\mu_1}{2}[(v^{-4}+2v^2-3)+a_1(v^{-8}-2v^{-4}+1)], & 0 \leqslant R < A, \\ \hat{W}^2(v) = \dfrac{\mu_2}{2}[(v^{-4}+2v^2-3)+a_2(v^{-8}-2v^{-4}+1)], & A < R \leqslant B, \end{cases} \tag{104}$$

where, from the considerations of Appendix A,

$$d^2\hat{W}^i(1)/dv^2 = 4\bar{E}^i = 4\mu_i(3+4a_i) > 0, \quad (i = 1, 2) \tag{105}$$

for this material. We recall from (71) that the $\bar{E}^i$ are Young's moduli in the radial direction.

On substitution from (104) into (83) and from (105) with $i = 1$ into (82), and making the definitions

$$\beta = \frac{\mu_2}{\mu_1}, \quad z(x) = (1+x^3)^{1/3}, \tag{106}$$

we find that (82)–(84) give the total energy for the composite sphere as

$$\Sigma(\rho) = \frac{1}{4(3+4a_1)}\left[\frac{\Phi(\rho)}{\mu_1} + \frac{p_0}{\mu_1}\Psi(\rho)\right], \tag{107}$$

where

$$\begin{aligned}\frac{\Phi(\rho)}{\mu_1} = \frac{3}{2}\Big\{&-\alpha^{-3}(\beta-1)[2z^2(\alpha\rho)-z^{-1}(\alpha\rho)-1]+\beta[2z^2(\rho)-z^{-1}(\rho)-1]\\ &-(\beta a_2-a_1)\Big[\tfrac{1}{3}\alpha^{-3}z^{-5}(\alpha\rho)+\tfrac{8}{3}\rho^3\Big(\tfrac{1}{5}z^{-5}(\alpha\rho)+\tfrac{1}{2}z^{-2}(\alpha\rho)\\ &-\frac{1}{\sqrt{3}}\arctan\frac{\sqrt{3}z(\alpha\rho)}{2+z(\alpha\rho)}-\frac{1}{\sqrt{3}}\arctan\frac{2z(\alpha\rho)+1}{\sqrt{3}}\Big)+\alpha^{-3}\Big(2z^{-1}(\alpha\rho)\\ &-\tfrac{8}{3}z^2(\alpha\rho)+\tfrac{1}{3}\Big)\Big]+\beta a_2\Big[\tfrac{1}{3}z^{-5}(\rho)+\tfrac{8}{3}\rho^3\Big(\tfrac{1}{5}z^{-5}(\rho)+\tfrac{1}{2}z^{-2}(\rho)-\frac{1}{\sqrt{3}}\arctan\frac{\sqrt{3}z(\rho)}{2+z(\rho)}\\ &-\frac{1}{\sqrt{3}}\arctan\frac{2z(\rho)+1}{\sqrt{3}}\Big)+2z^{-1}(\rho)-\tfrac{8}{3}z^2(\rho)+\tfrac{1}{3}\Big]+\frac{20\pi}{9\sqrt{3}}a_1\rho^3\Big\}\end{aligned} \tag{108}$$

and $\Psi(\rho)$ is given by (84). The details of the integration involved in (83) may be found in Polignone and Horgan (1993). Furthermore, from either (88) or (58), and making the definitions

$$\left.\begin{aligned}F[z(x)] &= z^{-1}(x)+\tfrac{1}{4}z^{-4}(x),\\ G[z(x)] &= F[z(x)]-\tfrac{1}{2}z^{-2}(x)-\tfrac{1}{5}z^{-5}(x)-\tfrac{1}{8}z^{-8}(x)\\ &\quad+\frac{1}{\sqrt{3}}\left[\arctan\frac{2z(x)+1}{\sqrt{3}}+\arctan\frac{\sqrt{3}z(x)}{2+z(x)}\right],\end{aligned}\right\} \tag{109}$$

we obtain the corresponding load/cavity relationship as

$$\begin{aligned}\frac{p_0(\rho)}{\mu_1} = 2z^2(\rho)\Big\{&(1-\beta)F[z(\alpha\rho)]+\beta F[z(\rho)]\\ &+2(\beta a_2-a_1)G[z(\alpha\rho)]-2\beta a_2 G[z(\rho)]+\frac{5\pi}{3\sqrt{3}}a_1\Big\}.\end{aligned} \tag{110}$$

For small values of ρ we have [see (59), (102) respectively]

$$\hat{p}(\rho) = \hat{p}_{cr} + K\rho^3 + o(\rho^3) \quad \text{as} \quad \rho^3 \to 0, \tag{111}$$

$$\Sigma(\rho) = -\tfrac{1}{2}K\rho^6 + o(\rho^6) \quad \text{as} \quad \rho^3 \to 0, \tag{112}$$

where, for the material at hand,

$$\hat{p}_{cr} = \frac{1}{4(3+4a_1)}\left[\frac{5}{2}+\left(\frac{40\pi-51\sqrt{3}}{30\sqrt{3}}\right)a_1\right] \quad \text{so that} \quad \frac{p_{cr}}{\mu_1} = \left[\frac{5}{2}+\left(\frac{40\pi-51\sqrt{3}}{30\sqrt{3}}\right)a_1\right] \tag{113}$$

and

$$K = \frac{2}{3}\left[\hat{p}_{cr} - \tfrac{1}{6}f^{-1} + \tfrac{1}{6}(f^{-1}-1)\beta\frac{(3+4a_2)}{(3+4a_1)}\right]. \tag{114}$$

We now examine the curve (110) and corresponding energy for the material (103) for large values of ρ. A detailed analysis of (110) shows that for large values of ρ,

$$\frac{p_0(\rho)}{\mu_1} \sim 2[\beta(1-\alpha^{-1})+\alpha^{-1}]\rho \quad \text{as} \quad \rho \to \infty, \tag{115}$$

while the expression for the energy on this curve for large ρ follows from (107), (108), (115) and (84) as

$$\frac{\varepsilon(\rho)}{\mu_1} \sim -3[\beta(1-\alpha^{-1})+\alpha^{-1}]\rho^2 \quad \text{as} \quad \rho \to \infty. \tag{116}$$

In (116), $\varepsilon(\rho)/\mu_1$ is defined to be the quantity in brackets in (107). The expressions (115), (116) are identical to those found by Horgan and Pence (1989a) for the composite neo-Hookean sphere. [See eqns (3.18), (3.19) of that reference; the additional factor of two in the equations in Horgan and Pence (1989a) is due to the authors' use of a shear modulus one-half that of the actual infinitesimal shear modulus.] Thus, the anisotropy considered here does not affect the large ρ asymptotic behavior of the bifurcation curve, nor the energy on it. Since $\alpha > 1, \beta > 0$ we see that $\beta(1-\alpha^{-1})+\alpha^{-1} > 0$. Thus, the curve (110) is asymptotic to a straight line with positive slope, while the energy will always be negative on this curve for sufficiently large values of ρ. Thus, the initial character of the bifurcation does not affect the large ρ asymptotic behavior. Note that we recover results for the homogeneous anisotropic sphere [see Polignone and Horgan (1993)] on setting $\alpha = 1$ in (115), (116).

In Figs 3–6 we have plotted the curve (110) for four different pairs of values of the anisotropy coefficients a_1, a_2, and the parameter ω defined in (64). [Note that for the material (103), we have

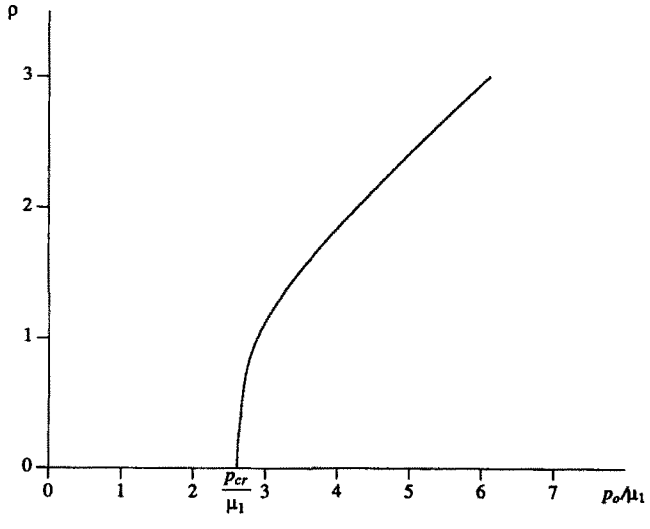

Fig. 3. Variation of the deformed cavity radius $\rho = c/B$ with applied dead-load traction p_0/μ_1 for the anisotropic composite sphere described by (103). Here $a_1 = 0.157$, $a_2 = 0.2477$, $\beta = (\mu_2/\mu_1) = 1.0$, $f = (A^3/B^3) = \alpha^{-3} = 0.1$, $\omega = [\mu_2(3+4a_2)]/[\mu_1(3+4a_1)] = 1.1$. Also $p_{cr}/\mu_1 = 2.61$.

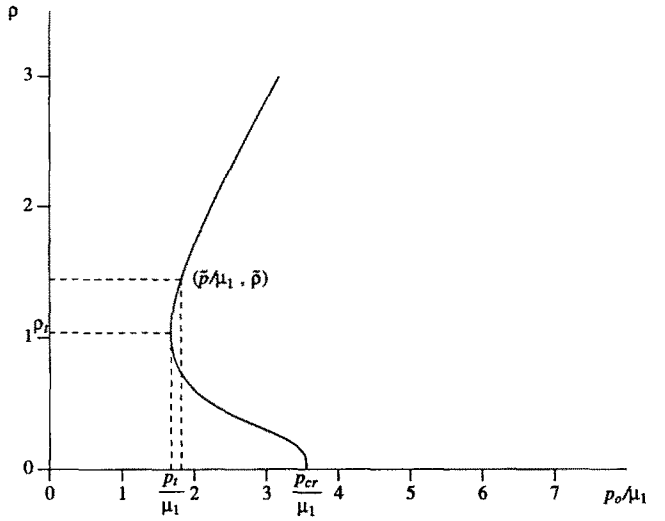

Fig. 4. Variation of the deformed cavity radius $\rho = c/B$ with applied dead-load traction p_0/μ_1 for the anisotropic composite sphere described by (103). Here $a_1 = 1.475$, $a_2 = 3.7$, $\beta = (\mu_2/\mu_1) = 0.1$, $f = (A^3/B^3) = \alpha^{-3} = 0.1$, $\omega = [\mu_2(3+4a_2)]/[\mu_1(3+4a_1)] = 0.2$. Also $p_{cr}/\mu_1 = 3.56$, $(p_t/\mu_1, \rho_t) = (1.68, 1.04)$, $(\tilde{p}/\mu_1, \tilde{\rho}) = (1.82, 1.45)$.

$$\omega = \beta \frac{(3+4a_2)}{(3+4a_1)} \tag{117}$$

so that choosing any three of the parameters in (117) specifies the last.] All graphs in Sections 6 and 7 correspond to a representative value $f = 0.1$ for the volume fraction of the core material to the total material. The situations corresponding to Figs 3 and 4 were discussed extensively by Horgan and Pence (1989a) and by Polignone and Horgan (1993). We will treat these briefly in what follows, and pay closer attention to the more novel phenomena displayed in Figs 5 and 6. In the case of Fig. 3, the composite sphere undergoes a bifurcation to the right and a smooth cavitation occurs. Here, an internal cavity is nucleated at the critical load, with its radius increasing continuously from zero as p_0 is

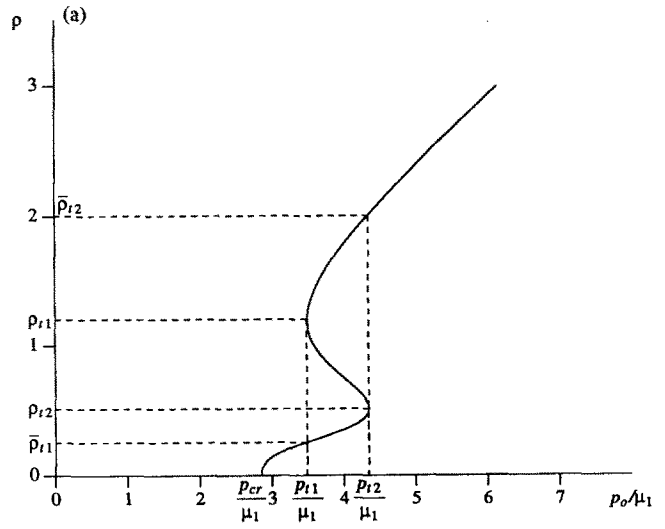

Fig. 5(a). Variation of the deformed cavity radius $\rho = c/B$ with applied dead-load traction p_0/μ_1 for the anisotropic composite sphere described by (103). Here $a_1 = 0.5$, $a_2 = 3.7$, $\beta = (\mu_2/\mu_1) = 1.0$, $f = (A^3/B^3) = \alpha^{-3} = 0.1$, $\omega = [\mu_2(3+4a_2)]/[\mu_1(3+4a_1)] = 3.56$. Also $p_{cr}/\mu_1 = 2.86$, $(p_{t1}/\mu_1, \rho_{t1}) = (3.49, 1.21)$, $(p_{t2}/\mu_1, \rho_{t2}) = (4.35, 0.52)$, $\bar{\rho}_{t1} = 0.25$, $\bar{\rho}_{t2} = 2.01$.

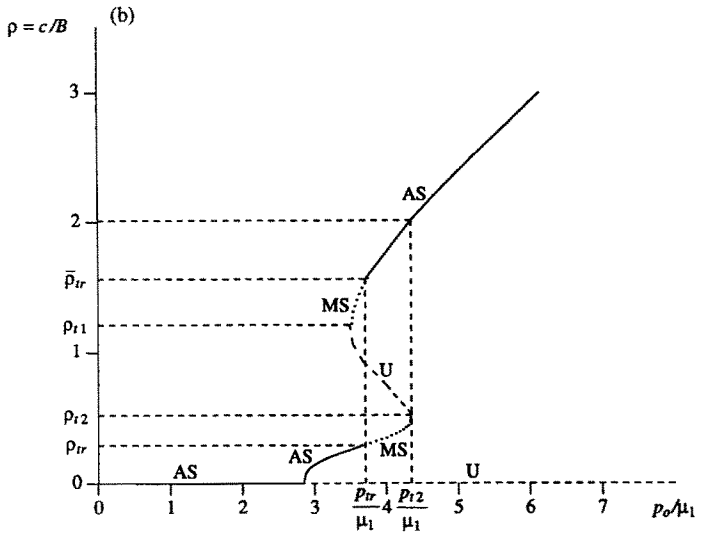

Fig. 5(b). Stability zones corresponding to bifurcation diagrams of the type displayed in Fig. 5(a). Here $a_1 = 0.5$, $a_2 = 3.7$, $\beta = (\mu_2/\mu_1) = 1.0$, $f = (A^3/B^3) = \alpha^{-3} = 0.1$, $\omega = [\mu_2(3+4a_2)]/[\mu_1(3+4a_1)] = 3.56$. Also $p_{tr}/\mu_1 = 3.71$, $\rho_{tr} = 0.29$, $\bar{\rho}_{tr} = 1.56$.

further increased. In Fig. 4, the composite sphere undergoes a bifurcation to the left. There exists a turning point (p_t, ρ_t) of the curve at which

$$\frac{dp_0}{d\rho} = 0, \tag{118}$$

and a cavity of finite radius is nucleated at a transition load $\tilde{p}$, with $p_t < \tilde{p} < p_{cr}$. The existence of a unique value $p = \tilde{p}$ was established by Horgan and Pence (1989a) for the composite neo-Hookean sphere, and the same result follows here from the Properties A and B given at the end of Section 5. Stability arguments of the type carried out in Horgan and Pence (1989a) and Polignone and Horgan (1993) again show that a "snap cavitation" occurs in which a discontinuous change in stable equilibrium configurations takes place.

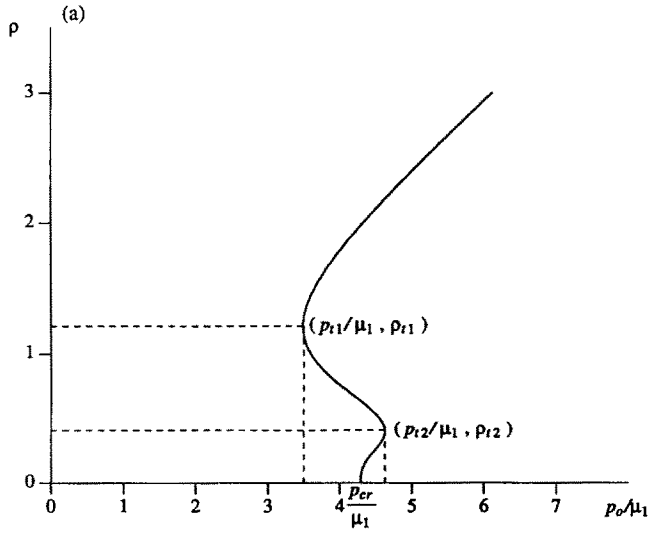

Fig. 6(a). Variation of the deformed cavity radius $\rho = c/B$ with applied dead-load traction p_0/μ_1 for the anisotropic composite sphere described by (103). Here $a_1 = 2.5$, $a_2 = 3.7$, $\beta = (\mu_2/\mu_1) = 1.0$, $f = (A^3/B^3) = \alpha^{-3} = 0.1$, $\omega = [\mu_2(3+4a_2)]/[\mu_1(3+4a_1)] = 1.37$. Also $p_{cr}/\mu_1 = 4.30$, $(p_{t1}/\mu_1, \rho_{t1}) = (3.50, 1.21)$, $(p_{t2}/\mu_1, \rho_{t2}) = (4.63, 0.41)$.

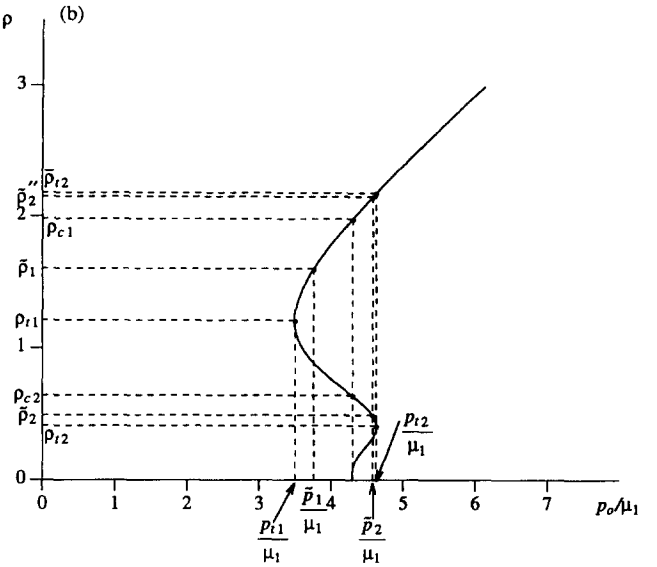

Fig. 6(b). Variation of the deformed cavity radius $\rho = c/B$ with applied dead-load traction p_0/μ_1 for the anisotropic composite sphere described by (103). Here $a_1 = 2.5$, $a_2 = 3.7$, $\beta = (\mu_2/\mu_1) = 1.0$, $f = (A^3/B^3) = \alpha^{-3} = 0.1$, $\omega = [\mu_2(3+4a_2)]/[\mu_1(3+4a_1)] = 1.37$. Also $(\tilde{p}_1/\mu_1, \tilde{\rho}_1) = (3.76, 1.60)$, $(\tilde{p}_2/\mu_1, \tilde{\rho}_2) = (4.58, 0.49)$, $\tilde{\rho}_{t2} = 2.18$, $\tilde{\rho}_2'' = 2.15$, $\rho_{c1} = 1.98$, $\tilde{\rho}_1 = 1.60$, $\rho_{c2} = 0.64$.

We consider now the situation in which the curve (110) bifurcates to the *right* from the trivial solution (86) at the point $(p_{cr}, 0)$, *and has two turning points* (p_{t1}, ρ_{t1}), (p_{t2}, ρ_{t2}), at which (118) holds. This is the case in Figs 5(a) and 6(a). In each of these figures, the curve (110) is monotonically increasing for $0 < \rho < \rho_{t2}$ and $\rho > \rho_{t1}$, and is monotonically decreasing for $\rho_{t2} < \rho < \rho_{t1}$. *Note that in Fig. 5(a),* p_{t1} *and* p_{t2} *both fall to the right of* p_{cr}, *while in Fig. 6(a),* p_{cr} *falls between* p_{t1} *and* p_{t2}.

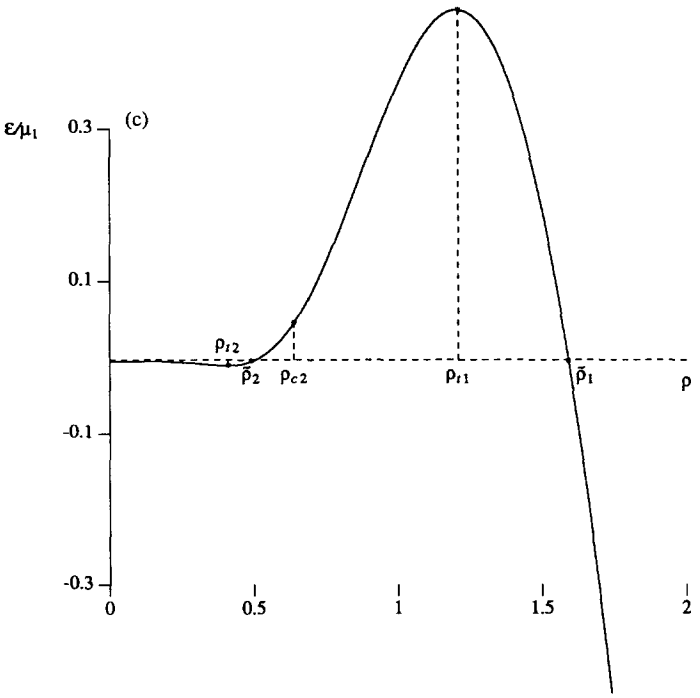

Fig. 6(c). Energy $[\varepsilon(\rho)/\mu_1] = [\Phi(\rho)/\mu_1] + [p_0(\rho)/\mu_1]\Psi(\rho)$, on the curve (110) for the parameter values of Fig. 6(a).

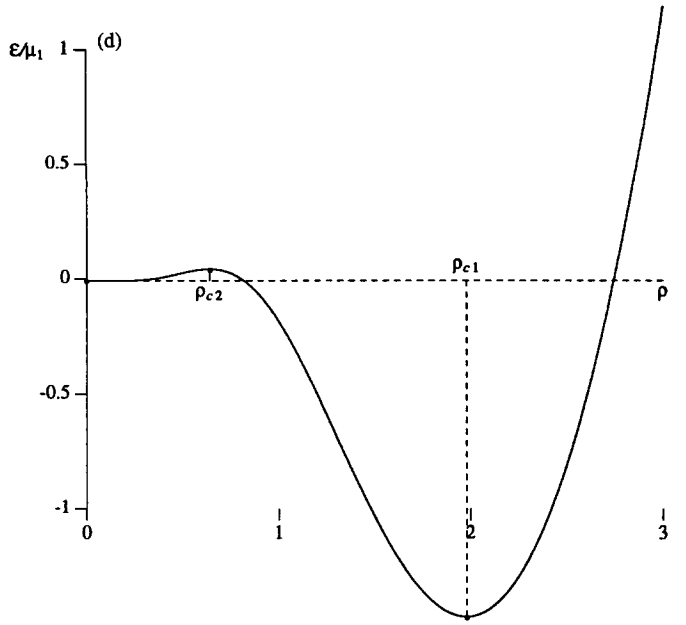

Fig. 6(d). Energy $[\varepsilon(\rho)/\mu_1] = [\Phi(\rho)/\mu_1] + [p_0/\mu_1]\Psi(\rho)$, for $p_0 = p_{cr}$ *fixed*, corresponding to the case of Fig. 6(a).

We first consider Fig. 5(a), for which the number of equilibrium solutions depends on the values of p_0 in the following way: for $0 < p_0 < p_{cr}$, the only solution is the trivial solution $\rho = 0$; for $p_{cr} < p_0 < p_{t1}$, there are exactly *two* solutions, namely, the trivial solution $\rho = 0$ and an additional bifurcated solution involving an internal cavity; for $p_{t1} < p_0 < p_{t2}$, there are exactly *four* solutions, namely, the trivial solution $\rho = 0$ and in addition three bifurcated solutions each involving an internal cavity; finally, for $p_0 > p_{t2}$, there are exactly *two* solutions, namely the trivial solution and a single bifurcated solution involving an internal cavity. The trivial solution provides a local minimum for Σ and hence is stable for $0 < p_0 < p_{cr}$, while for $p_0 > p_{cr}$ the trivial solution provides a local maximum for Σ and thus is unstable. By virtue of Property A, the bifurcated curve (110) provides a local maximum

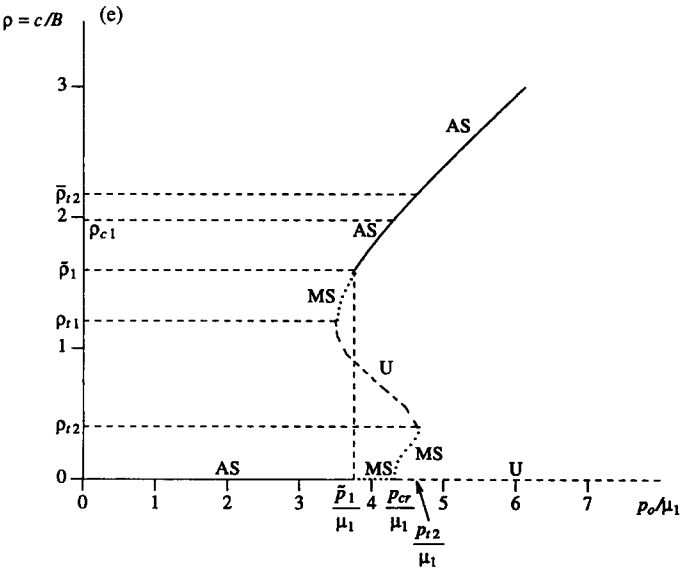

Fig. 6(e). Stability zones corresponding to bifurcation diagrams of the type displayed in Fig. 6(a). Here $a_1 = 2.5$, $a_2 = 3.7$, $\beta = (\mu_2/\mu_1) = 1.0$, $f = (A^3/B^3) = \alpha^{-3} = 0.1$, $\omega = [\mu_2(3+4a_2)]/[\mu_1(3+4a_1)] = 1.37$. Also $(\tilde{p}_1/\mu_1, \tilde{\rho}_1) = (3.76, 1.60)$, $(\tilde{p}_2/\mu_1, \tilde{\rho}_2) = (4.58, 0.49)$, $\bar{\rho}_{t2} = 2.18$, $\tilde{\rho}''_2 = 2.15$, $\rho_{c1} = 1.98$, $\tilde{\rho}_1 = 1.60$, $\rho_{c2} = 0.64$, $p_{t2}/\mu_1 = 4.63$.

for Σ if $\rho_{t2} < \rho < \rho_{t1}$ and hence the associated solution is unstable, while for $0 < \rho < \rho_{t2}$ and $\rho > \rho_{t1}$, this curve provides a local minimum for Σ and hence this solution is stable. Thus if $0 < p_0 < p_{t1}$ or if $p_0 > p_{t2}$, there is exactly one stable equilibrium solution, while if $p_{t1} < p_0 < p_{t2}$ there are two stable equilibrium solutions, each involving an internal cavity.

We now address the transition between metastability and absolute stability in the region $p_{t1} \leqslant p_0 \leqslant p_{t2}$. We again refer to Fig. 5(a). Observe that the stable branches on the region of interest correspond to the intervals $\bar{\rho}_{t1} \leqslant \rho \leqslant \rho_{t2}$ and $\rho_{t1} \leqslant \rho \leqslant \bar{\rho}_{t2}$, where $\bar{\rho}_{t1}$, $\bar{\rho}_{t2}$ are the points at which $p_0(\bar{\rho}_{t1}) = p_{t1}$, $p_0(\bar{\rho}_{t2}) = p_{t2}$, respectively, and where (118) is *not* satisfied. From Property B and $\Sigma(0) = 0$, we have that $\Sigma(\rho)$ decreases from zero on the interval $0 \leqslant \rho \leqslant \rho_{t2}$. Property B and (116) give that $\Sigma(\rho)$ is decreasing with ρ for $\rho > \rho_{t1}$, and $\Sigma(\rho)$ is negative for sufficiently large ρ. (Note that $\Sigma(\rho_{t1})$ can be either positive or negative.) We now define a transition load $p_0 = p_{tr}$, satisfying $p_{t1} \leqslant p_{tr} \leqslant p_{t2}$, such that for $p_{t1} \leqslant p_0 \leqslant p_{tr}$, we have $\Sigma(\rho)$ on $\bar{\rho}_{t1} \leqslant \rho \leqslant \rho_{tr}$ less than $\Sigma(\rho)$ on $\rho_{t1} \leqslant \rho \leqslant \bar{\rho}_{tr}$, and for $p_{tr} \leqslant p_0 \leqslant p_{t2}$, we have $\Sigma(\rho)$ on $\rho_{tr} \leqslant \rho \leqslant \rho_{t2}$ greater than $\Sigma(\rho)$ on $\bar{\rho}_{tr} \leqslant \rho \leqslant \bar{\rho}_{t2}$, where ρ_{tr}, $\bar{\rho}_{tr}$ ($\bar{\rho}_{tr} > \rho_{tr}$) are the values of ρ occurring on the stable branches for which $p_0(\rho) = p_{tr}$. In other words, p_{tr} is the value of the dead-load at which the energy on the upper portion of the bifurcation curve becomes less than that on the lower portion of this curve, and thus the value after which the upper branch remains the absolutely stable solution. The preceding is sketched in Fig. 5(b). Note that if $p_{tr} = p_{t1}$, then $\bar{\rho}_{tr} = \rho_{t1}$ and the upper branch is absolutely stable for $\rho > \rho_{t1}$, and if $p_{tr} = p_{t2}$, then $\rho_{tr} = \rho_{t2}$ and the lower branch is the absolutely stable solution for $0 < \rho \leqslant \rho_{t2}$.

Consider now the quasi-static loading process in which the composite sphere is subjected to a tensile dead-load surface traction p_0 which increases slowly from zero. We again refer to Fig. 5(b). The trivial homogeneous deformation (33) persists as p_0 is increased from zero, until the critical load, $p_0 = p_{cr}$, is reached. Then an internal void is nucleated, with cavity radius increasing continuously from zero as p_0 increases, until $p_0 = p_{tr}$. At this point there are two possibilities. First, if one supposes that the body always assumes an absolutely stable configuration, then as p_0 passes through p_{tr}, a discontinuous growth in cavity radius from $c = B\rho_{tr}$ to $c = B\bar{\rho}_{tr}$ is predicted, with cavity radius increasing continuously as p_0 is further increased. On the other hand, if one supposes that continuous deformation of the body persists as long as possible, then the cavity radius grows continuously as p_0 is increased until $p_0 = p_{t2}$ and then experiences a jump from $c = B\rho_{t2}$ to $c = B\bar{\rho}_{t2}$ as p_0 passes through p_{t2}. The cavity radius then increases continuously as p_0 is further increased. Note that the foregoing two possibilities coincide if $p_{tr} = p_{t2}$.

We next consider Fig. 6(a), for which the number of equilibrium solutions depends on the values of p_0 in the following way: for $0 < p_0 < p_{t1}$, the only solution is the trivial solution $\rho = 0$; for $p_{t1} < p_0 < p_{cr}$, there are exactly *three* solutions, namely, the trivial solution $\rho = 0$ and in addition two bifurcated solutions each involving an internal cavity; for $p_{cr} < p_0 < p_{t2}$, there are exactly *four* solutions, namely, the trivial solution $\rho = 0$ and in addition three bifurcated solutions each involving an internal cavity; finally, for $p_0 > p_{t2}$, there are exactly *two* solutions, namely the trivial solution and a single bifurcated solution involving an internal cavity. As noted earlier, the trivial solution provides a local minimum for Σ and hence is stable for $0 < p_0 < p_{cr}$, while for $p_0 > p_{cr}$ the trivial solution provides a local maximum for Σ and thus is unstable. Again by Property A, the bifurcated curve (110) provides a local maximum for Σ if $\rho_{t2} < \rho < \rho_{t1}$ and hence the associated solution is unstable, while for $0 < \rho < \rho_{t2}$ and $\rho > \rho_{t1}$, this curve provides a local minimum for Σ and hence this solution is stable. Thus if $0 < p_0 < p_{t1}$ or if $p_0 > p_{t2}$, there is exactly one stable equilibrium solution, while if $p_{t1} < p_0 < p_{cr}$ there are two stable equilibrium solutions, one involving an internal cavity, and if $p_{cr} < p_0 < p_{t2}$ there are two stable equilibrium solutions, each involving an internal cavity.

To address the transition between metastability and absolute stability, we refer to Figs 6(b, c), where ρ_{t1}, ρ_{t2}, p_{t1}, p_{t2} are as before, and ρ_{c1} denotes the value of $\rho > 0$ occurring on the stable branch for which $p_0(\rho) = p_{cr}$, while ρ_{c2} denotes the value of $\rho > 0$ such that $p_0(\rho) = p_{cr}$ occurs on the unstable branch. In Fig. 6(c) we have graphed the energy, $\varepsilon(\rho)/\mu_1 = [\Phi(\rho) + p_0(\rho)\Psi(\rho)]/\mu_1$, for $\rho > 0$ on the curve shown in Fig. 6(a). Note that the following analysis depends only on the sign of $\Sigma(\rho) = \varepsilon/[4\mu_1(3+4a_1)]$, which has the same

sign as ε so that all necessary information on Σ can be extracted from Fig. 6(c). We shall now show that there exists a unique value of p_0, namely $p_0 = \tilde{p}_1$, satisfying $p_{t1} < \tilde{p}_1 < p_{t2}$, such that, if $\tilde{p}_1 < p_{cr}$, the trivial solution is absolutely stable for $p_0 < \tilde{p}_1$, while for $p_0 > \tilde{p}_1$, the absolutely stable solution occurs on the bifurcated branch. [We note here that we shall confine attention to the case $\tilde{p}_1 < p_{cr}$ in what follows; stability for the case $\tilde{p}_1 > p_{cr}$ is analogous to the situation previously described for Fig. 5(b).] The desired result is established by the following argument: First, since $\Sigma(0) = 0$, we have $\Sigma(\rho_{t2}) < 0$ from Property B. Second, from Property A, we know that for $p_0 = p_{cr}$ fixed, $\rho = \rho_{c2}$ corresponds to a local maximum of the energy while $\rho = 0$ and $\rho = \rho_{c1}$ correspond to local minima. Thus, in particular, $\Sigma(\rho_{c2}) > \Sigma(0) = 0$. [We remark here that the energy curve *for fixed* p_0 is distinctly different from that displayed in Fig. 6(c). In Fig. 6(c), *every* value of ρ corresponds to a particular maximum or minimum of the energy associated with a corresponding value of the load p_0. To see this, compare Fig. 6(c) with Fig. 6(d), which represents the energy curve $\Sigma(\rho)$ vs ρ for fixed $p_0 = p_{cr}$. Figure 6(d) indeed shows that ρ_{c1}, ρ_{c2} correspond to extrema of the energy for p_0 fixed at $p_0 = p_{cr}$. Note also that although Fig. 6(d) implies $\Sigma(\rho_{c1}) < \Sigma(0) = 0$, this is not necessarily true for all curves of the type shown in Fig. 6(a).] Returning now to our argument, we have from $\Sigma(\rho_{t2}) < 0$, $\Sigma(\rho_{c2}) > 0$, and Property B, that there exists a unique value of $\rho = \tilde{\rho}_2$, satisfying $\rho_{t2} < \tilde{\rho}_2 < \rho_{c2}$, for which $\Sigma(\tilde{\rho}_2) = 0$ [see Fig. 6(c)]. We now consider the value of the load associated with $\tilde{\rho}_2$, defined to be $p_0(\tilde{\rho}_2) \equiv \tilde{p}_2$. Again from Property A for $p_0 = \tilde{p}_2$ fixed, $0 = \Sigma(\tilde{\rho}_2) > \Sigma(\tilde{\rho}_2'')$, where $\tilde{\rho}_2''$ is the largest value of ρ such that $p_0(\rho) = \tilde{p}_2$ [see Figs 6(b, c)]. We also observe that the above along with Property B give $\Sigma(\rho_{t1}) > 0$. Therefore, by Property B, there exists a unique value of $\rho = \tilde{\rho}_1$, satisfying $\rho_{t1} < \tilde{\rho}_1 < \tilde{\rho}_2''$, for which $\Sigma(\tilde{\rho}_1) = 0$. The associated load is then $p_0(\tilde{\rho}_1) \equiv \tilde{p}_1$ [see Figs 6(b, c)]. Thus, the energy on the bifurcated curve is such that $\Sigma(\rho) < 0$ for $0 < \rho < \tilde{\rho}_2$ and for $\rho > \tilde{\rho}_1$, while $\Sigma(\rho) > 0$ for $\tilde{\rho}_2 < \rho < \tilde{\rho}_1$. This completes the argument since the energy associated with the trivial solution is zero everywhere.

Consider now the previously envisioned quasi-static loading process. We thus refer to Fig. 6(e), where, as remarked earlier, we have $\tilde{p}_1 < p_{cr}$. If one supposes that the body always assumes an absolutely stable configuration, then the trivial homogeneous deformation (33) persists for $0 < p_0 < \tilde{p}_1$. As p_0 passes through $\tilde{p}_1$, the foregoing notion of stability predicts the sudden appearance of a cavity of finite radius $c = B\tilde{\rho}_1$. As p_0 is further increased, the cavity radius increases in a continuous fashion. On the other hand, one may suppose that the trivial homogeneous deformation (33) persists until it becomes unstable at $p_0 = p_{cr}$. *In this case, there are two possibilities as* p_0 *passes through* p_{cr}, similar to those discussed for Fig. 5(b). First, if one supposes that the body then assumes an absolutely stable configuration, the sudden appearance of a cavity of finite radius $c = B\rho_{c1}$ is predicted, with cavity radius increasing in a continuous fashion as p_0 is further increased. On the other hand, one may suppose that continuous deformation of the body persists as long as possible so that an internal void is nucleated at $p_0 = p_{cr}$ and the cavity radius grows continuously from zero until $p_0 = p_{t2}$ and then experiences a jump from $c = B\rho_{t2}$ to $c = B\tilde{\rho}_{t2}$, as p_0 passes through p_{t2}. The cavity radius then increases continuously as p_0 is further increased.

We have seen in the foregoing that there are *four* distinct types of bifurcation that can occur (Figs 3–6). Note that these four possibilities exist *regardless* of which of the schematic diagrams (Fig. 1 or Fig. 2) applies. In each of the diagrams, points in region II give rise to only *one* type of bifurcation (i.e. that shown in Fig. 4), while points in region I have three types of bifurcation associated with them (i.e. those shown in Figs 3, 5, 6). We also remark that although there corresponds a different diagram resembling either Fig. 1 or Fig. 2 *for every value of* a_1, these two diagrams exhaust the possibilities. For $a_1 < a_0$, we have a figure similar to Fig. 1, and for $a_1 > a_0$, we have a figure similar to Fig. 2. We recall from Polignone and Horgan (1993) that for a homogeneous sphere consisting of the inner material only, a_0 is the transition value of the anisotropy parameter, a, which governs whether bifurcation for this sphere is to the right ($a < a_0$) or to the left ($a > a_0$). The numerical value of $a_0 \approx 0.257$ is given by Polignone and Horgan (1993), eqn. (5.28). Finally, we observe that regardless of the stability criterion adopted, a discontinuous growth in cavity radius is predicted in three of the four types of bifurcation discussed.

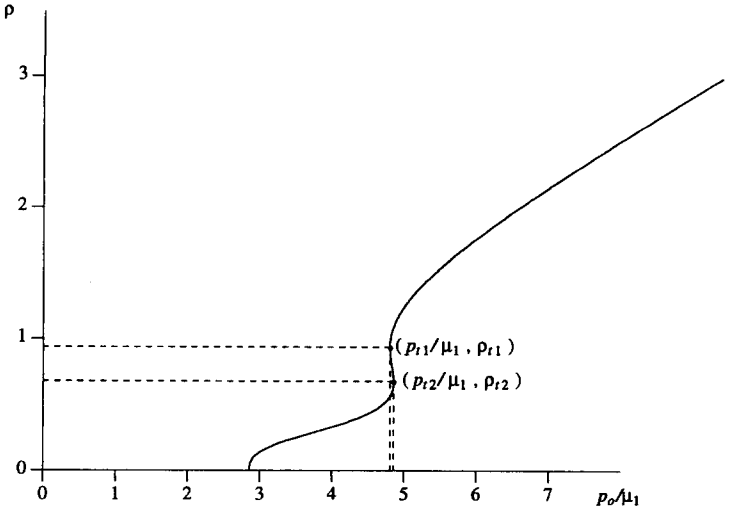

Fig. 7. Variation of the deformed cavity radius $\rho = c/B$ with applied dead-load traction p_0/μ_1 for the anisotropic composite sphere described by (103). Here $a_1 = 0.5$, $a_2 = 1.475$, $\beta = (\mu_2/\mu_1) = 2.0$, $f = (A^3/B^3) = \alpha^{-3} = 0.1$, $\omega = [\mu_2(3+4a_2)]/[\mu_1(3+4a_1)] = 3.56$. Also $p_{cr}/\mu_1 = 2.86$, $(p_{t1}/\mu_1, \rho_{t1}) = (4.81, 0.94)$, $(p_{t2}/\mu_1, \rho_{t2}) = (4.86, 0.68)$.

We conclude this section by addressing more closely how the anisotropy considered here results in the four different bifurcations we have seen. As stated above, when the parameter pair (ω, f) lies in region II in either of the schematic diagrams Figs 1, 2, we have seen only one type of bifurcation. However, when (ω, f) lies in region I, there are three possibilities. We now examine the role of the anisotropy parameters a_1, a_2, in determining which of the three types of bifurcation associated with region I occurs. For this purpose, we refer to Figs 5(a), 7 and 8. These three figures correspond to *the same value of* a_1, *the same parameter pair* (ω, f), *and different values of* a_2. Note that the value of β necessarily changes if one holds a_1 and ω fixed, and varies a_2 [see the comment following (117)]. As the value of a_2 is decreased from $a_2 = 3.7$ in Fig. 5(a), to $a_2 = 1.475$ in Fig. 7, the value of p_{t1} approaches that of p_{t2}, so that the region in which there is more than one stable solution, i.e. $p_{t1} \leqslant p_0 \leqslant p_{t2}$, becomes much smaller. When a_2 is further decreased to $a_2 = 0.14$ in Fig. 8, the curve (110) is monotone increasing, so that bifurcation here is of the type displayed in Fig. 3. We also note that, if we held the values of a_1, ω and f associated with Fig. 6(a) fixed and varied a_2 as above, this would give rise to figures similar to those shown in Figs

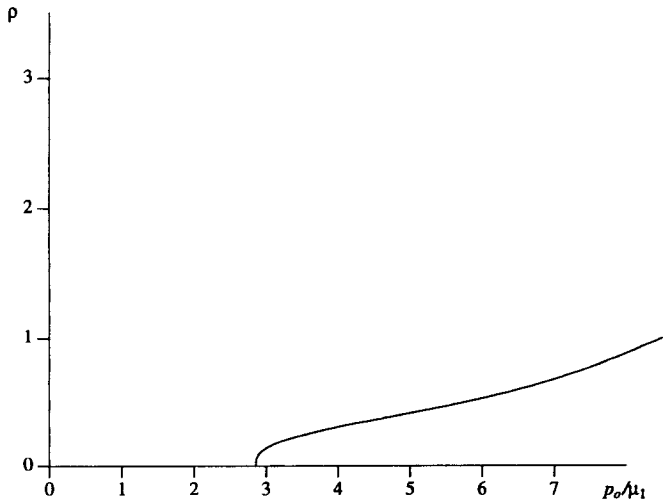

Fig. 8. Variation of the deformed cavity radius $\rho = c/B$ with applied dead-load traction p_0/μ_1 for the anisotropic composite sphere described by (103). Here $a_1 = 0.5$, $a_2 = 0.14$, $\beta = (\mu_2/\mu_1) = 5.0$, $f = (A^3/B^3) = \alpha^{-3} = 0.1$, $\omega = [\mu_2(3+4a_2)]/[\mu_1(3+4a_1)] = 3.56$. Also $p_{cr}/\mu_1 = 2.86$.

7 and 8. Thus, we conclude that it is the *magnitude of the anisotropy parameter* a_2 *associated with the surrounding shell* that is important in determining the region in which multiple stable solutions occur and thus the monotonicity of the curve (110). For large values of a_2 in the range $0 \leqslant a_2 \leqslant 5$, one obtains figures like Fig. 5(a) or Fig. 6(a), while for small a_2 one obtains figures like Fig. 8. In addition, we observe from Figs 5(a), 6(a) that the *magnitude of the anisotropy parameter* a_1 *associated with the core material* is also crucial in determining which of these two more novel types of bifurcation occurs. These two figures correspond to *the same values of* a_2, β *and* f, *but different values of* a_1 (and again, necessarily different values of ω). The above statement follows from the fact that the point at which the curve (110) bifurcates from the trivial solution, i.e. at $p_0/\mu_1 = p_{cr}/\mu_1$, is *solely* dependent upon the value of a_1 [see $(113)_2$ as well as the last paragraph of Section 4]. Thus, the magnitude of a_1 determines whether $p_{cr} < p_{t1}$ or $p_{cr} > p_{t1}$, which in turn implies whether we have a figure like Fig. 5(a) or Fig. 6(a), respectively. Finally, we observe that for a composite sphere corresponding to a diagram like that of Fig. 1, so that $a_1 < a_0 \approx 0.257$, the changes in character of the bifurcations are not as drastic as those associated with Fig. 2 since variations in the magnitude of a_1 are limited.

7. STRESS DISTRIBUTION

We proceed now to discuss the stress distribution in the composite anisotropic sphere. Recall that at the beginning of Section 3, we saw that the stresses corresponding to the trivial solution (32) were given as

$$T_{rr} = T_{\theta\theta} = T_{\phi\phi} = p_0. \tag{119}$$

Thus, prior to cavitation, we have simply the constant stress distribution (119). Subsequent to cavitation ($c > 0$), (45), (39), give the radial stress as

$$T_{rr}(R) = \int_{(1+c^3/R^3)^{1/3}}^{\infty} (v^3-1)^{-1} \hat{W}_1\left(v; \frac{c}{(v^3-1)^{1/3}}\right) dv, \quad \text{on} \quad 0 \leqslant R \leqslant B, \tag{120}$$

where we recall the notation (47), (48). On using (52), we may write (120) for the composite anisotropic sphere as

$$T_{rr}(R) = \begin{cases} \displaystyle\int_{(1+c^3/R^3)^{1/3}}^{\infty} (v^3-1)^{-1} \hat{W}_1^1(v)\, dv, & \text{on} \quad 0 \leqslant R \leqslant A, \\ p_0(1+c^3/B^3)^{-2/3} + \displaystyle\int_{(1+c^3/R^3)^{1/3}}^{(1+c^3/B^3)^{1/3}} (v^3-1)^{-1} \hat{W}_1^2(v)\, dv, & \text{on} \quad A \leqslant R \leqslant B. \end{cases} \tag{121}$$

Now, from (22), (23), (34), we can write the hoop stresses as

$$T_{\theta\theta}(R) = T_{\phi\phi}(R) = 2[(v^2-v^{-4})W_1|_R - (v^{-2}-v^4)W_2|_R - v^{-4}W_5|_R] + T_{rr}(R), \tag{122}$$

where $T_{rr}(R)$ is given by (120) or (121), and we recall the notation (40). From (121), (122) and our assumptions on the smoothness properties of W, we see that T_{rr} is a continuous function of R on $0 \leqslant R \leqslant B$, with a discontinuity in slope at the interface $R = A$, while $T_{\theta\theta}(R) = T_{\phi\phi}(R)$ suffers a jump discontinuity at the interface. The stress distributions (121),

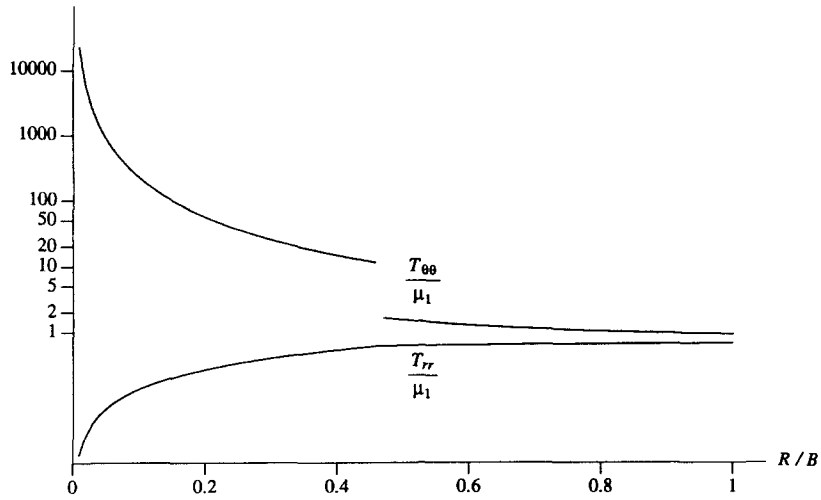

Fig. 9. Variation of the stresses $T_{rr}(R)$, $T_{\theta\theta}(R) = T_{\phi\phi}(R)$ with undeformed radius R subsequent to cavitation for the anisotropic composite sphere described by (103). The parameters are those corresponding to Fig. 4, i.e. $a_1 = 1.475$, $a_2 = 3.7$, $\beta = 0.1$, $\omega = 0.2$, $f = 0.1$. Also $p_0/\mu_1 = 1.85$, $p_{cr}/\mu_1 = 3.56$. At the material interface, the hoop stresses are discontinuous, and the radial stress is discontinuous in slope.

(122) are given explicitly [see (130), (131) below] for the material model (103) and are illustrated in Figs. 9 and 10. Further discussion of these figures will be carried out below.

Another interesting feature of the stresses immediately after cavitation is the presence of a boundary layer near the cavity wall in the case of smooth cavitation. To see this, we observe that for fixed $R, 0 < R \leqslant B$, letting $c \to 0+$ formally in (121) results in the right-hand side of (53), so that

$$\lim_{c \to 0+} T_{rr}(R) = p_{cr}, \quad 0 < R \leqslant B. \tag{123}$$

Since $T_{rr}(0) = 0$, (123) shows that, when smooth cavitation takes place (so that the cavity radius increases continuously from zero in a neighborhood of p_{cr}) the radial stress suffers a rapid growth near the cavity wall for applied dead loads p_0 slightly larger than p_{cr}. This boundary layer behavior is shown in Fig. 11 for a particular case of the material model (103). From (122), it is clear that a similar boundary layer exists in the stress components $T_{\theta\theta}(R)$, $T_{\phi\phi}(R)$.

We next consider the radial stress at the interface. From (121), we have

$$T_{rr}(A) = \int_{(1+c^3/A^3)^{1/3}}^{\infty} (v^3 - 1)^{-1} \hat{W}_1^1(v)\, dv. \tag{124}$$

We wish now to determine a sufficient condition on the strain-energy so that the maximum interfacial stress is reached at the point at which cavitation occurs. This will be the case if $T_{rr}(A)$ is monotone decreasing with respect to cavity radius $c > 0$. It is readily verified that

$$\frac{dT_{rr}(A)}{dc} = -\frac{1}{c}(1 + c^3/A^3)^{-2/3} \hat{W}_1^1(v)|_{v(A) = (1+c^3/A^3)^{1/3}} \tag{125}$$

so that for $c > 0$, $dT_{rr}(A)/dc < 0$ if and only if

$$\hat{W}_1^1(v) > 0 \quad \text{for all } v > 1. \tag{126}$$

Now, from (119), we have prior to cavitation,

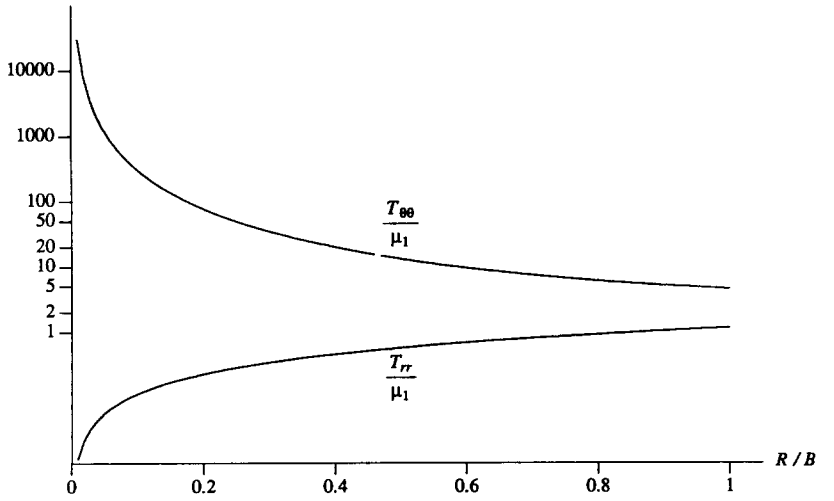

Fig. 10. Variation of the stresses $T_{rr}(R)$, $T_{\theta\theta}(R) = T_{\phi\phi}(R)$ with undeformed radius R subsequent to cavitation for the anisotropic composite sphere described by (103). The parameters are those corresponding to Fig. 6(a), i.e. $a_1 = 2.5$, $a_2 = 3.7$, $\beta = 1.0$, $\omega = 1.37$, $f = 0.1$. Also $p_0/\mu_1 = 3.95$, $p_{cr}/\mu_1 = 4.30$.

$$T_{rr}(A) = p_0, \quad c = 0, \tag{127}$$

and from (123), subsequent to cavitation,

$$\lim_{c \to 0+} T_{rr}(A) = p_{cr} \equiv \lim_{c \to 0+} p_0(c), \quad c > 0. \tag{128}$$

There are now three possibilities to consider. First, in the case of smooth cavitation, the radial stress at the interface $T_{rr}(A)$ increases linearly with p_0 until $p_0 = p_{cr}$, $T_{rr}(A)$ is

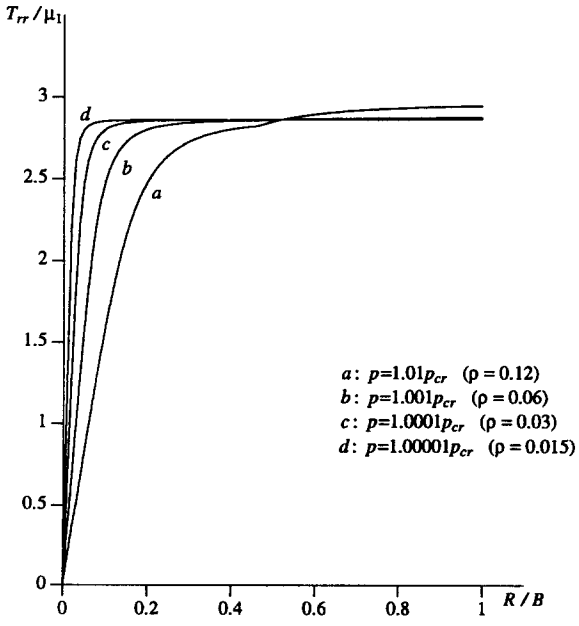

Fig. 11. Variation of the radial stress $T_{rr}(R)$, with undeformed radius R subsequent to cavitation for the anisotropic composite sphere described by (103). The parameters are those corresponding to Fig. 5(a), i.e. $a_1 = 0.5$, $a_2 = 3.7$, $\beta = 1.0$, $\omega = 3.56$, $f = 0.1$. Here $p_{cr}/\mu_1 = 2.86$. The radial stress is discontinuous in slope at the material interface.

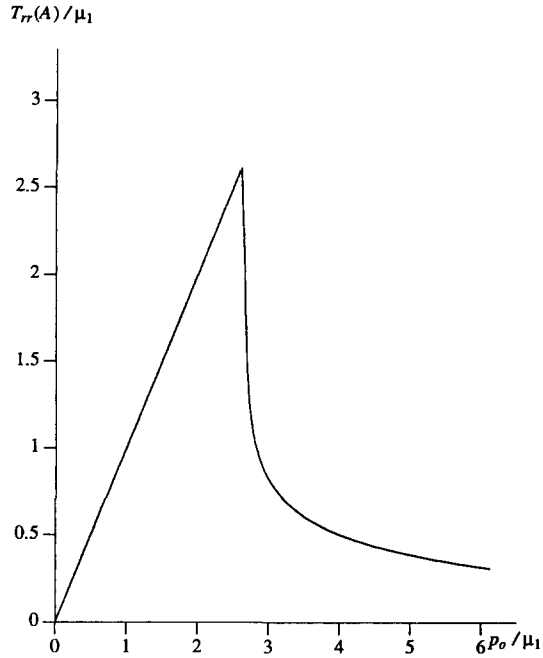

Fig. 12. Variation of the radial stress at the interface $T_{rr}(A)$ with applied dead load traction p_0/μ_1 for the anisotropic composite sphere described by (103) with parameters corresponding to Fig. 3, i.e. $a_1 = 0.157$, $a_2 = 0.2477$, $\beta = \mu_2/\mu_1 = 1.0$, $\omega = 1.1$, $f = 0.1$. Here $p_{cr}/\mu_1 = 2.61$.

continuous at $p_0 = p_{cr}$, and then decreases for $p_0 > p_{cr}$ (see Fig. 12). Second, for the case of snap cavitation, where a cavity of finite radius $c = c_0 > 0$ appears at a transition load $\tilde{p}_0 < p_{cr}$ ($\tilde{p}_0$ is analogous to the quantities $\tilde{p}$ or $\tilde{p}_1$ discussed in Section 6 in connection with Figs 4 or 6, respectively) eqn (128) is no longer relevant. The interfacial stress $T_{rr}(A)$ increases linearly with p_0 until $p_0 = \tilde{p}_0$, at which point it suffers a jump discontinuity. If condition (126) holds, it is easily seen that the integrand in (124) is positive on the range of integration, so that the jump in $T_{rr}(A)$ is negative. Thus upon appearance of a cavity with finite radius, ($c = c_0 > 0$, $p_0 = \tilde{p}_0$), the value of $T_{rr}(A)$ necessarily decreases (see Fig. 13). Third, consider the radial stress at the interface for the case in which the sphere undergoes a bifurcation of the type portrayed in Fig. 5. Here $T_{rr}(A)$ increases linearly with p_0 until $p_0 = p_{cr}$, $T_{rr}(A)$ is continuous at $p_0 = p_{cr}$, and decreases until p_0 reaches a transition value (greater than p_{cr}) where it again suffers a jump discontinuity (see Fig. 14).

As observed in Horgan and Pence (1989b), the foregoing considerations have immediate implications relating to the issue of possible debonding at the material interface $R = A$. (We remark that in that reference, a figure of the type displayed in Fig. 14 did not arise.) Suppose that the interface bond is sustained only so long as the normal stress at the interface remains less than a threshold value, T_d, a measure of the strength of the interface bond. Then debonding would occur if

$$T_{rr}(A) = T_d. \tag{129}$$

Consider again a quasi-static loading process in which p_0 increases slowly from zero. If $T_d < p_{cr}$ for smooth cavitation ($T_d < \tilde{p}_0$ for snap cavitation) then debonding occurs when $p_0 = T_d$ and cavitation is not relevant. However, if $T_d > p_{cr}$ for smooth cavitation ($T_d > \tilde{p}_0$ for snap cavitation), then when (126) holds, the resulting stress relief at the interface precludes the criterion (129) from being met and thus eliminates the possibility of interface debonding.

We conclude this section by returning to the material model (103). Recalling the notations (106) and (109), the stresses (121), (122) for a composite sphere composed of such a material can be written as

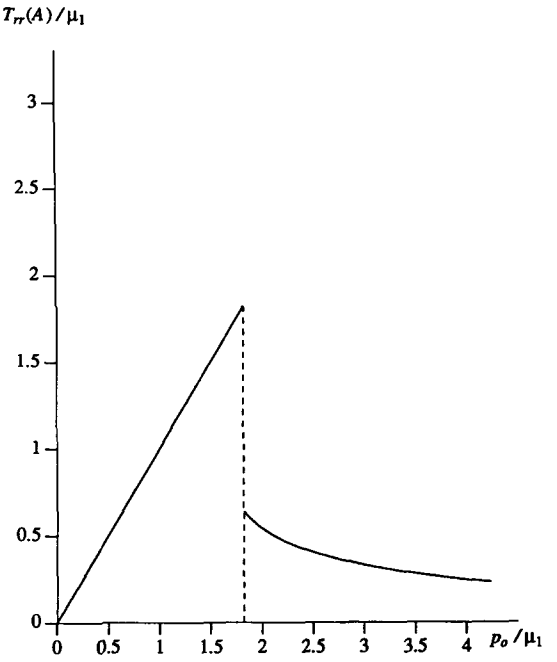

Fig. 13. Variation of the radial stress at the interface $T_{rr}(A)$ with applied dead load traction p_0/μ_1 for the anisotropic composite sphere described by (103) with parameters corresponding to Fig. 4, i.e. $a_1 = 1.475$, $a_2 = 3.7$, $\beta = \mu_2/\mu_1 = 0.1$, $\omega = 0.2$, $f = 0.1$. A jump discontinuity exists at $\tilde{p}/\mu_1 = 1.82$. Here $p_t/\mu_1 = 1.68$, $p_{cr}/\mu_1 = 3.560$.

$$\frac{T_{rr}(R)}{\mu_1} = \begin{cases} 2\left\{F\left[z\left(\frac{B}{R}\rho\right)\right] + 2a_1\left(\frac{5\pi}{6\sqrt{3}} - G\left[z\left(\frac{B}{R}\rho\right)\right]\right)\right\}, & 0 \leqslant R \leqslant A, \\ 2\left\{(1-\beta)F[z(\alpha\rho)] + \beta F\left[z\left(\frac{B}{R}\rho\right)\right] + \frac{5\pi}{3\sqrt{3}}a_1\right. \\ \quad \left. + 2(a_2\beta - a_1)G[z(\alpha\rho)] - 2a_2\beta G\left[z\left(\frac{B}{R}\rho\right)\right]\right\}, & A \leqslant R \leqslant B, \end{cases} \tag{130}$$

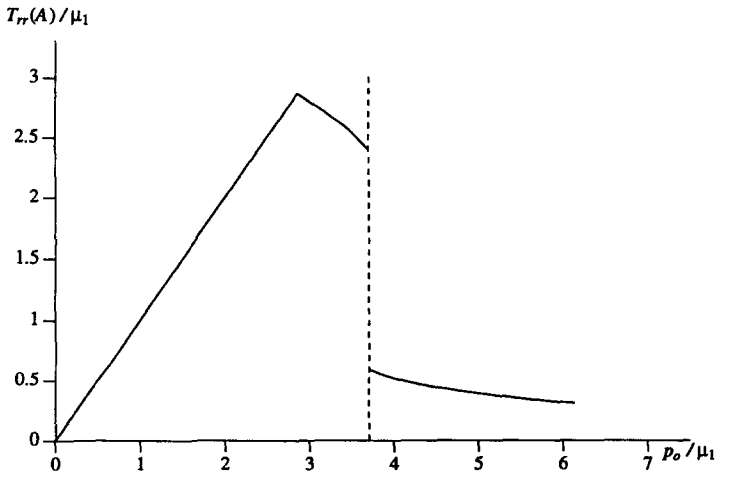

Fig. 14. Variation of the radial stress at the interface $T_{rr}(A)$ with applied dead load traction p_0/μ_1 for the anisotropic composite sphere described by (103) with parameters corresponding to Fig. 5(a), i.e. $a_1 = 0.5$, $a_2 = 3.7$, $\beta = 1.0$, $\omega = 3.56$, $f = 0.1$. A jump discontinuity exists at $p_{tr}/\mu_1 = 3.71$. Here $p_{t1}/\mu_1 = 3.49$, $p_{t2}/\mu_1 = 4.35$, $p_{cr}/\mu_1 = 2.86$.

and

$$\frac{T_{\theta\theta}(R)}{\mu_1} = \frac{T_{\phi\phi}(R)}{\mu_1} = \begin{cases} z^2\left(\frac{B}{R}\rho\right) - z^{-4}\left(\frac{B}{R}\rho\right) - 2a_1\left[z^{-8}\left(\frac{B}{R}\rho\right) - z^{-4}\left(\frac{B}{R}\rho\right)\right] + \frac{T_{rr}(R)}{\mu_1}, & 0 \leqslant R < A, \\ \beta\left[z^2\left(\frac{B}{R}\rho\right) - z^{-4}\left(\frac{B}{R}\rho\right)\right] - 2a_2\beta\left[z^{-8}\left(\frac{B}{R}\rho\right) - z^{-4}\left(\frac{B}{R}\rho\right)\right] + \frac{T_{rr}(R)}{\mu_1}, & A < R \leqslant B. \end{cases} \tag{131}$$

These stresses are shown in Figs 9 and 10 for parameter values corresponding to the bifurcation diagrams, Figs 4 and 6, respectively. In Fig. 9, these stresses are plotted for a case with $\beta < 1$ ($\mu_2 < \mu_1$). When $\beta > 1$ ($\mu_2 > \mu_1$), the jump in $T_{\theta\theta} = T_{\phi\phi}$ at the material interface $R = A$ is in the opposite direction to that in Fig. 9, while the slope discontinuity in T_{rr} has the opposite character. In Fig. 10, we have $\beta = 1.0$, and the jump discontinuity in $T_{\theta\theta} = T_{\phi\phi}$ nearly vanishes. This dependence of the hoop stress discontinuity on the relative sizes of μ_1, μ_2, i.e. on the size of β compared to unity, was seen in the hoop stresses corresponding to the composite neo-Hookean sphere discussed in Horgan and Pence (1989b). Thus, the anisotropy considered here has a negligible effect on the jump discontinuity in the hoop stresses at the material interface. This can be seen from (131) since it is the βz^2 term in the second of (131) which contributes most significantly to the discontinuity.

Finally, it is easily verified that the condition (126) holds for the material (103), so that we *do have* normal stress relaxation at the material interface subsequent to cavitation for all materials of the type (103). Thus, as seen earlier, regardless of the stability criterion adopted, there are essentially three possible ways in which the composite sphere may deform. First, a smooth cavitation may take place. Second, an immediate snap cavitation at some load *less than* the critical load may occur. Third, a smooth cavitation may initially take place, followed by a "snap" from one finite cavity radius to another at some load *greater than* the critical load. The interfacial normal stress for these three cases are shown in Figs 12, 13 and 14 for spheres with parameter values corresponding to the bifurcation diagrams, Figs. 3, 4, and 5(a), respectively.

Acknowledgements—This research was supported in part by the National Science Foundation under Grant No. MSS-91-02155, by the U.S. Air Force Office of Scientific Research under Grant No. AFOSR-F49620-92-J-0112, and by the U.S. Army Research Office under Grant No. DAAL 03-91-G-0022. The research of D. A. Polignone was also supported by a National Defense Science and Engineering Graduate Fellowship (NDSEGF) awarded by the U.S. Air Force.

REFERENCES

Abeyaratne, R. and Hou, H.-s. (1989). Growth of an infinitesimal cavitiy in a rate-dependent solid. *J. Appl. Mech.* **56,** 40–46.

Abeyaratne, R. and Hou, H.-s. (1991a). Void collapse in an elastic solid. *J. Elasticity* **26,** 23–42.

Abeyaratne, R. and Hou, H.-s. (1991b). On the occurrence of the cavitation instability relative to the asymmetric instability under symmetric dead-load conditions. *Q. J. Mech. Appl. Math.* **44,** 429–449.

Antman, S. S. and Negrón-Marrero, P. V. (1987). The remarkable nature of radially symmetric equilibrium states of aeolotropic nonlinearly elastic bodies. *J. Elasticity* **18,** 131–164.

Ball, J. M. (1982). Discontinuous equilibrium solutions and cavitation in nonlinear elasticity. *Phil. Trans. Roy. Soc. Lond.* **A306,** 557–610.

Chou-Wang, M.-S. and Horgan, C. O. (1989a). Void nucleation and growth for a class of incompressible nonlinearly elastic materials. *Int. J. Solids Structures* **25,** 1239–1254.

Chou-Wang, M.-S. and Horgan, C. O. (1989b). Cavitation in nonlinear elastodynamics for neo-Hookean materials. *Int. J. Engng Sci.* **27,** 967–973.

Chung, D.-T., Horgan, C. O. and Abeyaratne, R. (1986). The finite deformation of internally pressurized hollow cylinders and spheres for a class of compressible elastic materials. *Int. J. Solids Structures* **22,** 1557–1570.

Chung, D.-T., Horgan, C. O. and Abeyaratne, R. (1987). A note on a bifurcation problem in finite plasticity related to void nucleation. *Int. J. Solids Structures* **23,** 983–988.

Ertan, N. (1988). Influence of compressibility and hardening on cavitation. *ASCE J. Engng Mech.* **114,** 1231–1244.

Eubanks, R. A. and Sternberg, E. (1954). On the axisymmetric problem of elasticity theory for a medium with transverse isotropy. *J. Rat. Mech. Anal.* **3,** 89–101.
Gent, A. N. (1990). Cavitation in rubber: A cautionary tale. *Rubber Chem. Technol.* **63,** G49–G53.
Gent, A. N. and Lindley, P. B. (1958). Internal rupture of bonded rubber cylinders in tension. *Proc. Roy. Soc. Lond.* **A249,** 195–205.
Haughton, D. M. (1986). On non-existence of cavitation in incompressible elastic membranes. *Q. J. Mech. Appl. Math.* **39,** 289–296.
Haughton, D. M. (1990). Cavitation in compressible elastic membranes. *Int. J. Engng Sci.* **28,** 163–168.
Horgan, C. O. (1992), Void nucleation and growth for compressible nonlinearly elastic materials: an example. *Int. J. Solids Structures* **29,** 279–291.
Horgan, C. O. and Abeyaratne, R. (1986). A bifurcation problem for a compressible nonlinearly elastic medium: Growth of a micro-void. *J. Elasticity* **16,** 189–200.
Horgan, C. O. and Pence, T. J. (1989a). Void nucleation in tensile dead-loading of a composite incompressible nonlinearly elastic sphere. *J. Elasticity* **21,** 61–82.
Horgan, C. O. and Pence, T. J. (1989b). Cavity formation at the center of a composite incompressible nonlinearly elastic sphere. *J. Appl. Mech.* **56,** 302–308.
Horgan, C. O. and Pence, T. J. (1989c). Void nucleation due to large deformations in nonlinearly elastic composites. *Proc. 4th Japan–US Conference on Composite Materials*, Washington, DC, June 1988 (Edited by J. R. Vinson), pp. 232–241. Technomic Publishing Co., Lancaster, PA.
Hou, H.-s. and Abeyaratne, R. (1992). Cavitation in elastic and elastic–plastic solids. *J. Mech. Phys. Solids* **40,** 571–592.
Hou, H.-s. and Zhang, Y. (1990). The effect of axial stretch on cavitation in an elastic cylinder. *Int. J. Nonlin. Mech.* **25,** 715–722.
Huang, Y., Hutchinson, J. W. and Tvergaard, V. (1991). Cavitation instabilities in elastic–plastic solids. *J. Mech. Phys. Solids* **39,** 223–242.
James, R. D. and Spector, S. J. (1991). The formation of filamentary voids in solids. *J. Mech. Phys. Solids* **39,** 783–814.
Jaunzemis, W. (1967). *Continuum Mechanics*. Macmillan, New York.
Meynard, F. (1992). Existence and nonexistence results on the radially symmetric cavitation problem. *Q. Appl. Math.* **50,** 201–226.
Pericak-Spector, K. A. and Spector, S. J. (1988). Nonuniqueness for a hyperbolic system: Cavitation in nonlinear elastodynamics. *Arch. Rat. Mech. Anal.* **101,** 293–317.
Podio-Guidugli, P., Vergara Caffarelli, G. and Virga, E. G. (1986). Discontinuous energy minimizers in nonlinear elastostatics: An example of J. Ball revisited. *J. Elasticity* **16,** 75–96.
Polignone, D. A. and Horgan, C. O. (1993). Cavitation for incompressible anisotropic nonlinearly elastic spheres. *J. Elasticity* (in press).
Sivaloganathan, J. (1986a). Uniqueness of regular and singular equilibria for spherically symmetric problems of nonlinear elasticity. *Arch. Rat. Mech. Anal.* **96,** 97–136.
Sivaloganathan, J. (1986b). A field theory approach to stability of radial equilibria in nonlinear elasticity. *Math. Proc. Camb. Phil. Soc.* **99,** 589–604.
Sivaloganathan, J. (1991). Cavitation, the incompressible limit, and material inhomogeneity. *Q. Appl. Math.* **49,** 521–541.
Spencer, A. J. M. (1972). *Deformations of Fibre-reinforced Materials*. Oxford University Press, Oxford.
Spencer, A. J. M. (1982). The formulation of constitutive equations for anisotropic solids. In *Mechanical Behavior of Anisotropic Solids (Proceedings of Euromech Colloquium 115)* (Edited by J.-P. Boehler), pp. 3–26. Martinus Nijhoff, The Hague.
Steigmann, D. J. (1992). Cavitation in elastic membranes—an example. *J. Elasticity* **28,** 277–287.
Stuart, C. A. (1985). Radially symmetric cavitation for hyperelastic materials. *Ann. Inst. Henri Poincaré-Analyse non lineaire* **2,** 33–66.
Stuart, C. A. (1993). Estimating the critical radius for radially symmetric cavitation. *Q. Appl. Math.* **51,** 251–263.
Tian-hu, H. (1990). A theory of the appearance and growth of the micro-spherical void. *Int. J. Fract.* **43,** R51–R55.
Tvergaard, V. (1990). Material failure by void growth to coalescence. In *Advances in Applied Mechanics* (Edited by J. Hutchinson and T. Wu), Vol. 27, pp. 83–151. Academic Press, San Diego.
Tvergaard, V., Huang, Y. and Hutchinson, J. W. (1992). Cavitation instabilities in a power hardening elastic-plastic solid. *European J. Mech. A (Solids)* **11,** 215–232.
Walker, J. L. (1956). Structure of ingots and castings. In *Liquid Metals and Solidification*, pp. 319–336. American Society for Metals, Cleveland.
Williams, M. L. and Schapery, R. A. (1965). Spherical flaw instability in hydrostatic tension. *Int. J. Fract. Mech.* **1,** 64–71.

APPENDIX A

(i) *Verification of (70)*

We first show how $d^2\hat{W}(1)/dv^2$ is related to the elastic moduli for infinitesimal deformations and thereby establish (70). Denoting by w the strain-energy density for an incompressible *linearly* elastic material which is transversely isotropic about an axis along the unit vector $\mathbf{a}$, we have [see e.g. Spencer (1982)]

$$w = \mu_T \operatorname{tr} \mathbf{E}^2 + 2(\mu_L - \mu_T)\mathbf{a}\cdot\mathbf{E}^2\cdot\mathbf{a} + \tfrac{1}{2}\beta(\mathbf{a}\cdot\mathbf{E}\cdot\mathbf{a})^2, \tag{A1}$$

where β, μ_T, μ_L are elastic constants, and $\mathbf{E}$ is the infinitesimal strain tensor. For the deformations of concern here, we find that

$$w = w(v) = \mu_T[(v^{-2}-1)^2+2(v-1)^2]+2(\mu_L-\mu_T)(v^{-2}-1)^2+\tfrac{1}{2}\bar{\beta}(v^{-2}-1)^2. \tag{A2}$$

From (A2), it is readily verified that

$$\frac{d^2w(1)}{dv^2} = 4(\bar{\beta}-\mu_T+4\mu_L). \tag{A3}$$

For infinitesimal deformations of the nonlinear material with strain-energy $\hat{W}(v)$ given by (47) (where the second argument in (47) has been suppressed), it is natural to assume that $[d^2\hat{W}(1)/dv^2] = [d^2w(1)/dv^2]$, and so from (A3) we find that

$$\frac{d^2\hat{W}(1)}{dv^2} = 4(\bar{\beta}-\mu_T+4\mu_L), \tag{A4}$$

which is (70).

(ii) *Verification of (71)*

To show the result (71), we first consider the strain-energy density function for a linearly elastic transversely isotropic *compressible* material, given by Spencer (1982) as

$$\tilde{w} = \tfrac{1}{2}\lambda(\mathrm{tr}\,\mathbf{E})^2+\mu_T\,\mathrm{tr}\,\mathbf{E}^2+\bar{\alpha}(\mathbf{a}\cdot\mathbf{E}\cdot\mathbf{a})\,\mathrm{tr}\,\mathbf{E}+2(\mu_L-\mu_T)\mathbf{a}\cdot\mathbf{E}^2\cdot\mathbf{a}+\tfrac{1}{2}\bar{\beta}(\mathbf{a}\cdot\mathbf{E}\cdot\mathbf{a})^2, \tag{A5}$$

where λ, μ_T, μ_L, $\bar{\alpha}$ and $\bar{\beta}$ are elastic constants, and $\mathbf{a}$, $\mathbf{E}$ are as defined above.

Alternatively, when $\mathbf{a} = (1,0,0)$, one may write the above in the following form [see Eubanks and Sternberg (1954)]:

$$\tilde{w} = \tfrac{1}{2}a(E_{22}^2+E_{33}^2)+\tfrac{1}{2}\bar{a}E_{11}^2+(a-2\bar{\mu})E_{22}E_{33}+b(E_{22}+E_{33})E_{11}+2\mu(E_{12}^2+E_{13}^2)+2\bar{\mu}E_{23}^2, \tag{A6}$$

where the E_{ij} $(i,j = 1,2,3)$ are components of the infinitesimal strain tensor $\mathbf{E}$, and a, $\bar{a}$, b, μ and $\bar{\mu}$ are elastic constants, with μ and $\bar{\mu}$ shear moduli. In Eubanks and Sternberg (1954), it is also given that $\bar{E}_C$, the Young's Modulus in the direction of transverse-isotropy (the 1-direction) for a *compressible* linearly elastic transversely-isotropic material, is

$$\bar{E}_C = \frac{a\bar{a}-b^2-\overline{a\mu}}{a-\bar{\mu}} \tag{A7}$$

[see eqn (3.12) of the above reference]. On comparing (A5) with (A6) and using (A7), we find $\bar{E}_C$ expressed in terms of the parameters associated with (A5) to be

$$\bar{E}_C = \frac{(\lambda+\mu_T)(\lambda-2\mu_T+\bar{\beta}+4\mu_L+2\bar{\alpha})-(\lambda+\bar{\alpha})^2}{(\lambda+\mu_T)} \tag{A8}$$

$$= \frac{\lambda(\bar{\beta}-\mu_T+4\mu_L)+\mu_T(\bar{\beta}+4\mu_L-2\mu_T+2\bar{\alpha})-\bar{\alpha}^2}{(\lambda+\mu_T)}. \tag{A9}$$

To now recover the desired result for an *incompressible* linearly elastic transversely-isotropic material, we let $\lambda \to \infty$ in (A9) [see Spencer (1972), pp. 91–92]. Thus, on using l'Hopital's Rule we obtain

$$\bar{E} \equiv \lim_{\lambda\to\infty}\bar{E}_C = \bar{\beta}-\mu_T+4\mu_L, \tag{A10}$$

which is the desired result (71).

(iii) *Verification of (105)*

On comparing (A4) with (A10), we obtain

$$\frac{d^2\hat{W}(1)}{dv^2} = 4\bar{E} > 0, \tag{A11}$$

where the inequality in (A11) is required for positive definiteness of w [see e.g. Eubanks and Sternberg (1954), p. 96]. Specializing to our composite sphere, we have from (A10), (A11),

$$\frac{d^2\hat{W}^i(1)}{dv^2} = 4\bar{E}^i = 4(\bar{\beta}^i-\mu_T^i+4\mu_L^i) > 0, \quad (i = 1,2), \tag{A12}$$

where the superscripts $i = 1,2$ correspond to the core and outer materials, respectively.

For the material model (103), (104), it is easily seen that

$$\frac{d^2\hat{W}^i(1)}{dv^2} = 4\mu_i(3+4a_i) > 0, \quad (i = 1,2), \tag{A13}$$

where the inequality follows from (A11). By reasoning analogous to that given at the end of part (i) of this Appendix, we have the desired result (105) on equating (A12) and (A13). We remark finally that as we have

$\mu_i > 0$, eqn (A13) requires $a_i > -\frac{3}{4}$, a somewhat less restrictive condition than our assumption of non-negative a_i made just after (103).

APPENDIX B

(i) *Verification of (85)*

Here we present the details of the derivation of (85). Recall from (82) and $(64)_4$ that

$$\Sigma(\rho) = \frac{\Phi(\rho)}{d^2\hat{W}^1(1)/dv^2} + \hat{p}\Psi(\rho), \quad \rho \geqslant 0, \tag{B1}$$

where $\Phi(\rho)$, $\Psi(\rho)$ are given by (83), (84), respectively. From (84), it is easily seen on taking derivatives that

$$\dot{\Psi}(0+) = \ddot{\Psi}(0+) = 0, \quad \dddot{\Psi}(0+) = -6. \tag{B2}$$

We thus confine attention to the evaluation of $\dot{\Phi}$, $\ddot{\Phi}$, $\dddot{\Phi}$ as $\rho \to 0+$ to establish the desired results.

(ii) *Verification of* $\dot{\Sigma}(0+) = 0$

By the chain-rule, we have $\dot{\Phi}(\rho) = 3\rho^2\, d\Phi/d\rho^3$, where $d\Phi/d\rho^3$ is given by (93), so that

$$\dot{\Phi}(0+) = \lim_{\rho \to 0+} 3\rho^2\, d\Phi/d\rho^3 = 0, \tag{B3}$$

where we have used (98) in the final step in (B3). From (B1) we have

$$\dot{\Sigma}(\rho) = \frac{\dot{\Phi}(\rho)}{d^2\hat{W}^1(1)/dv^2} + \hat{p}\dot{\Psi}(\rho), \tag{B4}$$

so that upon evaluation of (B4)as $\rho \to 0+$ and substitution from $(B2)_1$, (B3), we have the desired result $(85)_1$, i.e.

$$\dot{\Sigma}(0+) = 0. \tag{B5}$$

(iii) *Verification of* $\ddot{\Sigma}(0+) = 0$

By the chain-rule, we have

$$\ddot{\Phi}(\rho) = 6\rho\frac{d\Phi}{d\rho^3} + 9\rho^4\frac{d^2\Phi}{d(\rho^3)^2}, \tag{B6}$$

where again the first derivative on the right is given by (93), and the second by (99). Substituting (99) into (B6) and taking the limit as $\rho \to 0+$ gives

$$\ddot{\Phi}(0+) = \lim_{\rho \to 0+} 6\rho\frac{d\Phi}{d\rho^3} + \lim_{\rho \to 0+} 3\rho\left[\frac{\hat{W}_1^2((1+\alpha^3\rho^3)^{1/3}) - \hat{W}_1^1((1+\alpha^3\rho^3)^{1/3})}{(1+\alpha^3\rho^3)^{2/3}} - \frac{\hat{W}_1^2(1+\rho^3)^{1/3})}{(1+\rho^3)^{2/3}}\right], \tag{B7}$$

where we note from an argument analogous to that used in (B3) that the first term on the right in (B7) is zero. It is shown in Polignone and Horgan (1993) that $\hat{W}_1^i(1) = 0$, $(i = 1, 2)$, and so the second term in (B7) is also zero. Thus,

$$\ddot{\Phi}(0+) = 0. \tag{B8}$$

From (B4) we have

$$\ddot{\Sigma}(\rho) = \frac{\ddot{\Phi}(\rho)}{d^2\hat{W}^1(1)/dv^2} + \hat{p}\ddot{\Psi}(\rho), \tag{B9}$$

so that upon evaluation of (B9) as $\rho \to 0+$ and substitution from $(B2)_2$, (B8), we have the desired result $(85)_2$, i.e.

$$\ddot{\Sigma}(0+) = 0. \tag{B10}$$

(iv) *Verification of* $\dddot{\Sigma}(0+) = 6(\hat{p}_{cr} - \hat{p})$

By the chain-rule, it can be shown that

$$\dddot{\Phi}(\rho) = 6\frac{d\Phi}{d\rho^3} + 54\rho^3\frac{d^2\Phi}{d(\rho^3)^2} + 27\rho^6\frac{d^3\Phi}{d(\rho^3)^3}. \tag{B11}$$

From (98), we know that the limit as $\rho \to 0+$ of the first term on the right in (B11) is $6p_{cr}$, so that the desired result will follow from showing that the last two terms in (B11) are zero as $\rho \to 0+$. We first address the second term on the right in (B11). It is easily seen that, on substitution from (99) and on using $\hat{W}_1^i(1) = 0$, $(i = 1, 2)$, we have

$$\lim_{\rho \to 0+} 54\rho^3 \frac{d^2\Phi}{d(\rho^3)^2} = 0. \tag{B12}$$

To address the last term in (B11), we first differentiate (99) to obtain

$$\frac{d^3\Phi}{d(\rho^3)^3}(\rho) = \frac{1}{3}\left\{\frac{\frac{1}{3}\alpha^3\rho^3[d^2\hat{W}^2/dv^2 - d^2\hat{W}^1/dv^2]((1+\alpha^3\rho^3)^{1/3})}{\rho^6(1+\alpha^3\rho^3)^{4/3}}\right.$$
$$- \frac{\left(\frac{2}{3}\alpha^3\rho^3(1+\alpha^3\rho^3)^{-1/3} + (1+\alpha^3\rho^3)^{2/3}\right)[\hat{W}_1^2 - \hat{W}_1^1]((1+\alpha^3\rho^3)^{1/3})}{\rho^6(1+\alpha^3\rho^3)^{4/3}}$$
$$\left. - \frac{\frac{1}{3}\rho^3\frac{d^2\hat{W}^2}{dv^2}((1+\rho^3)^{1/3}) + \left(\frac{2}{3}\rho^3(1+\rho^3)^{-1/3} + (1+\rho^3)^{2/3}\right)\hat{W}_1^2((1+\rho^3)^{1/3})}{\rho^6(1+\rho^3)^{4/3}}\right\}, \tag{B13}$$

where, in (B13) we have introduced the notation

$$[f-g](x) \equiv f(x) - g(x). \tag{B14}$$

Since the quantities $d^2\hat{W}^i(1)/dv^2$ $(i = 1, 2)$, are finite, substitution from (B13) into the last term in (B11) and taking the limit as $\rho \to 0+$ results in

$$\lim_{\rho \to 0+} 27\rho^6 \frac{d^3\Phi}{d(\rho^3)^3} = 0. \tag{B15}$$

Thus, we have shown that the last two terms on the right in (B11) vanish as $\rho \to 0+$ and so

$$\bar{\Phi}(0+) = 6p_{cr}. \tag{B16}$$

From (B9) we have

$$\bar{\Sigma}(\rho) = \frac{\bar{\Phi}(\rho)}{d^2\hat{W}^1(1)/dv^2} + \hat{p}\bar{\Psi}(\rho), \tag{B17}$$

so that upon evaluation of (B17) as $\rho \to 0+$ and substitution from $(B2)_3$, (B16), we have [recalling $(64)_3$] the desired result $(85)_3$, i.e.

$$\bar{\Sigma}(0+) = 6(\hat{p}_{cr} - \hat{p}). \tag{B18}$$